

RC1:

This paper applied the WRF-CMAQ model to simulate the air quality over the Beijing-Tianjin-Hebei area and calculate the trans-boundary fluxes to Beijing, Tianjin, and Shijiazhuang. This paper used a new method that assessed the pollutants transport by vertical surface flux calculation instead of usually used scenario analysis.

Author's reply: We feel encouraged to receive the reviewer's recognition for our work. We treasure the valuable comments raised by the referee and have followed them in revising the manuscript. Please check the below for the point-to-point responses.

(1) Using this method, it is easily to understand the pollutants inflows from each direction or each surrounding city to the objective city. But the inflows from one city didn't necessarily mean those pollutants were from that city. It might be generated from the upflow cities. Did the authors consider about that? And is there any consideration about solving this?

Authors' reply: We appreciate for the valuable comment. Indeed, the transport flux itself could not tell whether the pollutants are from the neighbor city or from other upstream cities, and this problem is one of the major disadvantages of the flux method. However, the goal of using the flux method is mainly focused on the transport from different directions, rather than the contribution of different cities. By putting together the transport characteristics of different cities as is done in our study (see Fig. R1), we have obtained a general transport feature in the BTH region, which can facilitate a qualitative understanding of where the fluxes are mainly from.

As shown in Fig. R1, in January, the PM_{2.5} that flows into Beijing from Baoding on the southeast mainly happens at a higher level, so the PM_{2.5} may origin from a larger area upstream. Then we can track backward along the dark arrow, and the inflow may come from Baoding, Shijiazhuang or even Xingtai. In July, the transport directions between Baoding and Shijiazhuang are different at the lower and the upper level. We can infer that the inflowing PM_{2.5} into Shijiazhuang mainly come from Baoding rather than farther regions to the northeast.

We admit that the flux approach cannot quantitatively evaluate the contribution from each city, and we hope that future studies can combine the flux method with other methods such as tagging models to quantitatively assess the contribution of different cities or regions on the transport pathways identified in the current study.

We have included the preceding discussions on the limitations in the revised manuscript. (Page 15, Line 401-407)

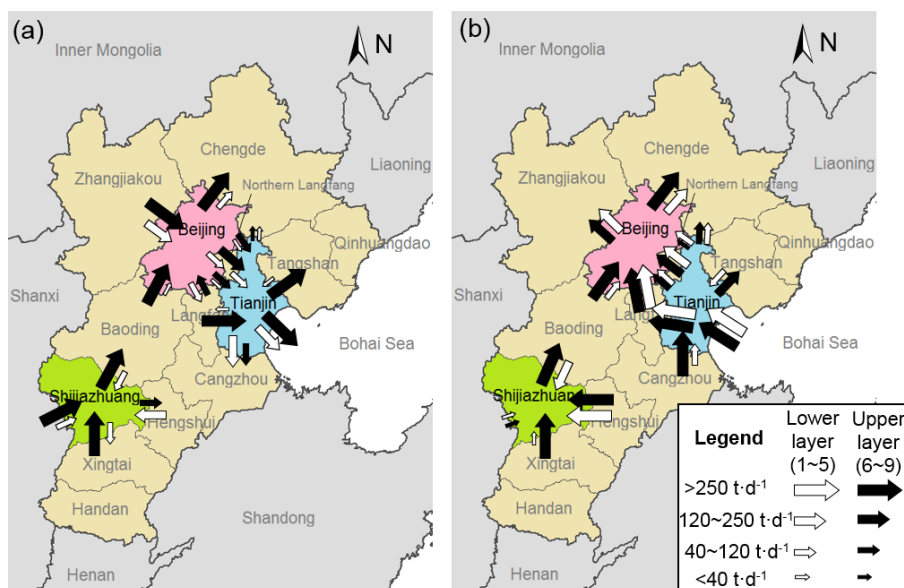


Figure R1 The transport fluxes through each boundary segment of the three target cities in January (a) and July (b). The size of the arrows represents the amount of the fluxes, while white and black arrows denote fluxes at the lower (layer 1-5 in the model, from the ground to about 310 m) and upper (layer 6-9 in the model, from about 310 m to about 1000 m) layers, respectively.

(2) Wind directions are very important to calculate the pollutants fluxes (Figure 3 and Equation 1). But in the model evaluation section (S2), the authors only evaluate the wind speed, temperature, and humidity. I would suggest the authors to evaluate the wind direction in the simulation results.

Authors' reply: We thank the referee for the good suggestion. We evaluated the wind direction using the same method as the other meteorology parameters. The results are shown in Table R1. The bias of wind direction at 10m (WD10) falls within the benchmark, but the gross error exceeds the benchmark for both January and July. The larger gross error is partly caused by the lower precision of the observation data. The WD10 observations only have 16 different values, while the simulation could have any value between 0 and 360. For example, if the real WD10 is 125 degree, the value will be reported as 140 degree. Even if the simulation is exactly 125 degree, an additional gross error of 15 degree will be introduced. In addition, compared to other similar simulation studies in China (e.g., Hu et al., 2016; Zhao et al., 2013), the gross error of WD10 falls in a similar range. Therefore, we still believe that the simulated meteorology field shows a reasonable agreement with the observation.

We have added the data and the discussion above in our SI (Page 3, Line 37 – 50).

Table R1 Comparison of simulated and observed wind direction

Parameter	Index	Unit	Benchmark ^a	Jan-2012	Jul-2012
Wind direction (WD10)	Observation Mean	deg	-	203.9	175.2
	Simulation Mean	deg	-	222.4	174.8
	Bias	deg	$\leq \pm 10$	-2.64	-1.47
	Gross error	deg	≤ 30	43.23	43.7

a. The benchmarks used in this study are suggested by Emery (2011).

RC2:

This paper analyzed the flux flow between cities in BTH area, northern plain in China, with a commonly used transport model WRF-CMAQ. It is an important issue for policy makers to understand the regional transport of air pollution, and would be helpful in decision of emission control strategy. The paper is clearly written and easy to follow. I suggest its publication when the following issues are further stressed or discussed.

Author's reply: We appreciate the reviewer's valuable comments which help us improve the quality of the manuscript. We have carefully revised the manuscript according to the reviewers' comments. Below is our point-to-point responses to the issues raised by the reviewer.

(1) Language. There are some grammar errors in the manuscript and the language should be polished.

Authors' reply: We sincerely apologize for the deficiency in language. We have gone through the text carefully and corrected the grammar errors.

(2) Lines 56-57, Page 3. It is not quite persuasive, since the non-linear relationship is considered in the DDM and RSM methods.

Authors' reply: We thank the referee for pointing out the problem. The expression in the manuscript was not quite accurate and might cause misunderstanding. We believe that all methods based on chemical transport models, including the DDM and RSM methods, are able to consider the non-linear relationship between emissions and concentrations. However, the sensitivity of PM_{2.5} concentrations to emission perturbation, which DDM and RSM aim to quantify, is different from the inter-city transport of PM_{2.5}. Assuming that the emission reduction in the source region leads to a 30% reduction in PM_{2.5} concentration in the target region, the transboundary transport of PM_{2.5} may not be 30% because of the nonlinearity in the emission-concentration relationships.

Zhao et al (2017) found that during winter time, the PM_{2.5} could response negatively to NO_x reduction. Therefore, if we use sensitivity approach such as brute-force method,

DDM and RSM to assess the regional transport of PM_{2.5}, the result may deviate (probably underestimate) from the real case.

We changed our expression in the manuscript for a better understanding of the insufficiency of the DDM and RSM methods for our study (Page 3, Line 55-57).

(3) Lines 128-129, Page 6. The authors stated that the biases of simulated meteorological field and PM_{2.5} concentrations fall in a reasonable range. For meteorological field, the statement could be supported by Table S1, with the evidence by Emery et al., 2001. For PM_{2.5} concentrations, however, we could not think it is "reasonable" as no further information is given. The bias could be quite large in some case, and some major components such as SOC were largely underestimated as indicated by the authors. Therefore, I suggest that the authors provide the evidence or criterion to justify the model performance., or describe the current simulation progress (model performance) in BTH region.

Authors' reply: We thank the referee for the valuable suggestion. We calculated additional indices including Mean Fractional Bias (MFB) and Mean Fractional Error (MFE), and compared them with the benchmark values suggested by Boylan and Russell (2006). The definition of the two indices can also be found in the research of Boylan and Russell (2006). The simulation results of the PM_{2.5} concentration are well within the model performance criteria. We have added the new statistical results as well as the benchmark values in Table 2 in the manuscript.

Due to the limitation of monitoring sites, the benchmark is not applicable for the evaluation of PM_{2.5} components. Therefore, we compare the model performance with other studies in the BTH region. The results are summarized in Table R2. All of the studies underestimate the sulfate concentrations. The underestimation ranges between 9% and 79%, and most of them are larger than 30%. The nitrate simulation results vary in different studies, but the majority of the studies tend to overestimate its concentration. The concentration of EC is usually much lower than the other four components, which may contribute to the large discrepancy in the simulation results in different studies. For OC, although some studies overestimate the concentration, more studies exhibit a lower concentration than observation. Generally speaking, the biases of the PM_{2.5} components in the current study have similar magnitude to other recent studies in the BTH region.

We have included the discussion in the revised SI (Page 7, Line 69-80)

Table R2 Summary of the PM_{2.5} component simulation results for the BTH region in recent studies

Time	Site	SO ₄ ²⁻	NO ₃ ⁻	NH ₄ ⁺	EC	OC	Reference
		NMB (%)	NMB (%)	NMB (%)	NMB (%)	NMB (%)	
2005 annual	Tsinghua, Beijing	-14	13	10	-24	-36	Wang et al., 2011
2005 annual	Miyun, Beijing	-36	62	9	-17	-52	Wang et al., 2011
14 Jan – 8 Feb, 2010	Beijing	-72	-32	-5	124	26	Liu et al., 2016
14 Jan – 8 Feb, 2010	Shangdianzi, Beijing	-78	-24	-13	36	-7	Liu et al., 2016
Jan, 2010	Peking university, Beijing	-39	85	33	101	-2	Liu et al., 2016
14 Jan – 8 Feb, 2010	Shijiazhuang, Hebei	-79	-35	-7	81	38	Liu et al., 2016
14 Jan – 8 Feb, 2010	Chengde, Hebei	-78	48	-10	-39	-50	Liu et al., 2016
14 Jan – 8 Feb, 2010	Tianjin	-72	0	9	149	85	Liu et al., 2016
11-15 Jan, 2013	Beijing	~ -73	~ -43	-	-	-	Wang et al., 2014
Jan 2013	Handan, Hebei	-9	33	-11	50	37	Wang et al., 2015
Jul 2013	Handan, Hebei	-32	-3	8	96	30	Wang et al., 2015
Oct – Nov, 2014	7 sites in the BTH region	-48	16	-25	87	-37	Zhao et al., 2017
22 Jul – 23 Aug, 2012	Xiong County, Hebei	-52	95	2	120	-25	This study
22 Jul – 23 Aug, 2012	Ling County, Shandong	-57	79	-14	117	-1	This study

(4) Section 3.2, Page 9. The authors described the difference in flux pattern between Jan and July. However, the reasons for the difference is not further discussed, and the seasonal mechanisms in pollution transport remained unclear. More information should be provided here.

Authors' reply: We appreciate for the valuable comment. What determine the seasonal transport flux are mainly two factors, the wind speed and the PM_{2.5} concentration in the upstream areas. The PM_{2.5} concentration is related to both the meteorology condition and the emission, with the upstream emissions being the most important factor. If we understand the roles of emissions and winds in the transport, we can answer the question of the seasonal mechanisms. Therefore, we combined the response of this comment with the fifth one below.

(5) Related with Q4, the paper described the pattern of pollution transport between cities, which is helpful for policy making. For scientific issue, however, the main factors influencing the transport were not sufficiently discussed. Could the author explain the roles of emissions and meteorological condition on the transport using the cases presented in the paper?

Authors' reply: We combine the response of this comment with the fourth one. To better understand how the wind and concentration affect the transport fluxes, we have made several wind rose plots for different cities, different seasons and different heights. Besides the traditional wind rose plot that displays wind direction with wind speed frequencies, we also made plots that display the wind direction with PM_{2.5}

concentration frequencies. We chose the ground layer and the 7th layer to represent the lower layer and the upper layer respectively. The plots for Beijing are shown in Fig. R2 as an example. The plots for the other two cities are displayed in the SI (Fig. S3 and Fig. S4).

In January, the dominant wind directions near the ground ranges from northwest to northeast. The NNE wind has the highest frequency, while the NW wind has the highest wind speed (Fig. R2(a)). The dominant northern winds reflect the winter monsoon. Although the concentration coming with the northern winds are relatively low because of the low emission rate on that direction (Fig. R2(b)), the high frequency and wind speed also cause an overall strong transport from the northwest to the southeast. Wind directions and the corresponding concentrations are quite different at the upper layers (Fig. R2(c), (d)). The prevalent northern wind remains (though the dominant directions shift slightly from NNE to NW), and the frequency of southwestern winds is much higher than that at lower layers. Moreover, the PM_{2.5} concentrations that come with southwestern winds are much higher than the other directions. The strong emission in southern Hebei (which lies on the southwest direction of Beijing), especially the elevated sources may be responsible for the high concentration from the southwest. Therefore, in January, the dominant northwestern winds account for the Northwest-Southeast pathway at both lower layers and upper layers, while the large emissions on the southwest direction mainly caused the Southwest-Northeast pathway at upper layers. In July, the dominant wind directions at the lower layer are the southeastern directions, reflecting the summer monsoon (Fig R2(e)), and coincidentally the highest concentrations also come along with the southeastern winds (Fig R2(f)). Emissions from Tianjin, Langfang, and Tangshan may influence Beijing by the southeastern winds. The emission and the wind direction both contribute to the Southeast-Northwest pathway at the lower layers. The high frequency wind directions shift clockwise to the southern directions at the upper layers in July, as is shown in Fig. R2(g), and the southwest wind and the southeast wind are both important. Moreover, the directions with high concentrations also shift to both the southwest and the southeast directions (Fig. R2(h)). Therefore, in July, the dominant southeastern winds and the emissions on the southeast directions caused the Southeast-Northwest pathway at both the upper and the lower layers. The Southwest-Northeast pathway is a combination result from the southern winds and the emissions, which is different from that in January.

Similar analysis can be made to the plots for the other two cities. Due to the length limitation, we put the plots into the SI. The plots in Fig. R2 and the discussions above has been included in our revised manuscript (Page 10-11, Line 262-287).

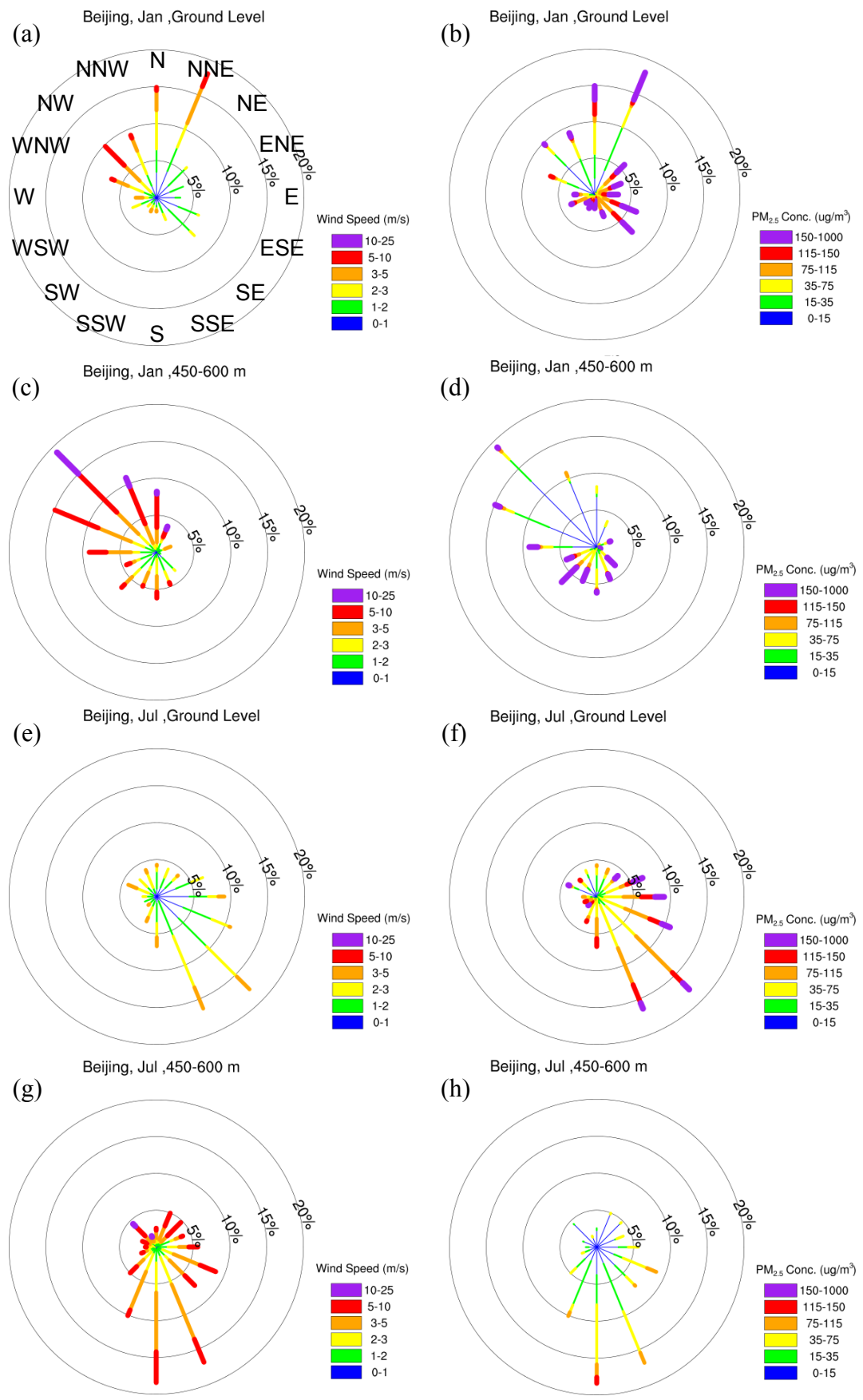


Figure R2 The wind rose plots showing the frequency of wind speed (a, c, e, g) and PM_{2.5}

concentration (b, d, f, h) at different wind directions for Beijing. The ground level and the 7th level (about 450-600 m) in the model are chosen to represent lower levels and upper levels. The percentages denote the frequency.

SC1:

The manuscript is meaningful for the prevention and control of regional pollution in north China. It is absolutely worth of publishing as the study itself is extremely interesting. However, some improvements are suggested.

Authors' reply: It is our honor to receive the valuable comments from Dr. Tang. We have revised the manuscript carefully according to these comments. Please see below for our point-to-point responses.

In the manuscript, the authors found the southwest-northeast transport pathway. Actually, it is the most important pathway in North China Plain, especially during the heavy polluted episodes. Tang et al. (2015) and Zhu et al. (2016) found aerosols transported from the southwest between 500-1200 m (in the upper boundary layer) using ceilometer observations, which were the same with your simulations. However, the transport just emerged during the initial periods of the heavy pollution episodes. With the increase of the aerosols, the PBL decreases (below 500m) and the transport effects weaken during the heavy polluted periods. Could you please quantify the transport in different pollution degrees?

Authors' reply: The reviewer raised a very useful question. The transport fluxes vary with different meteorology conditions in different days. Following this suggestion, we calculated the flux for individual days in January and July, and sorted the data into groups based on different pollution levels (see Fig. R3). Taking Beijing as an example, in January, the simulated concentration ranges from 11 $\mu\text{g}/\text{m}^3$ to 271 $\mu\text{g}/\text{m}^3$, while in July, the range is from 6 $\mu\text{g}/\text{m}^3$ to 94 $\mu\text{g}/\text{m}^3$. We set 6 groups for January and 5 groups for July. The separating points are chosen to be near the 30, 55, 75, 85 and 95 percentiles in January, and the 30, 60, 80, 90 percentiles in July. The groups are denser at higher concentrations to better reveal the details before and after heavy pollution periods.

In January, the transport becomes stronger when the concentration is higher, but the transport flux decreases in turn when the concentration is the highest. The inflow from Baoding and outflow to Chengde, which are the indicator of the Southwest-Northeast pathway, also experience a gradual rise followed by a sudden decline. In July, the situation is similar, though the decrease is less significant. Such result is consistent with Tang et al. (2015) and Zhu et al. (2016) that the Southwest-Northeast transport pathway is more significant during the rising phase of a heavy pollution period, but fades when the pollution reaches the peak.

Inspired by these results, we also conducted a day-to-day analysis on the two heavy pollution episodes described in Section 3.3, which occur in January and July, respectively (Fig. R4). We find the "flowing in and accumulating" phenomenon for both episodes. For the episode in January, the inflow (especially from southwest) is

strong in January 18th, while the inflow declines rapidly in January 19th, the day with the highest concentration. The phenomenon is more significant during the episode in July. In July 18th and 19th, the inflow flux is very strong, while in July 20th which has the highest concentration, the flux decreases for more than one order of magnitude. This finding emphasizes the importance of early temporary control before heavy pollution occurs. We have revised our manuscript to include the above results and discussions. (Page 11-12, Line 294-306)

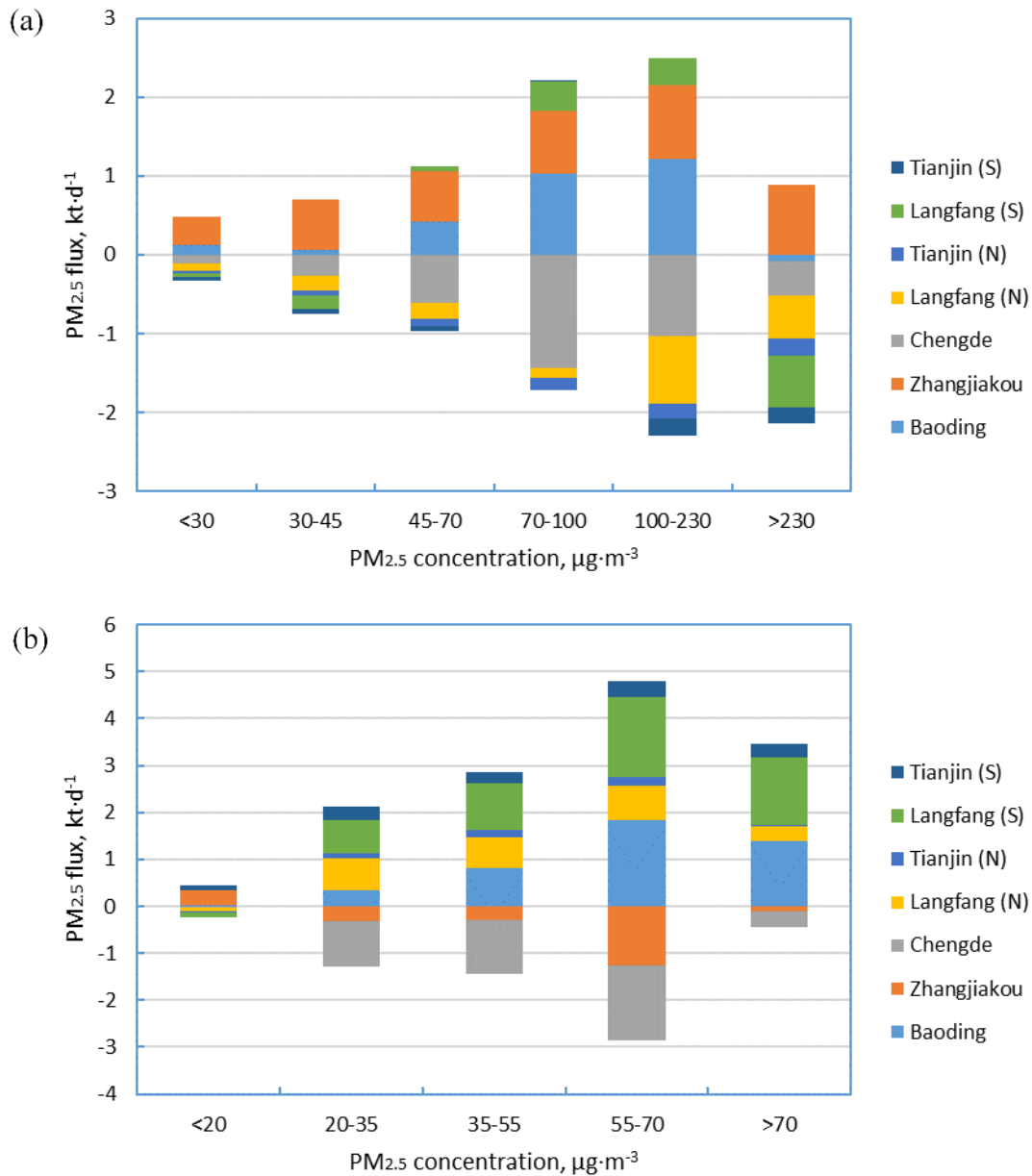


Figure R3 PM_{2.5} average flux between Beijing and its neighboring cities in different pollution degrees in (a) January and (b) July.

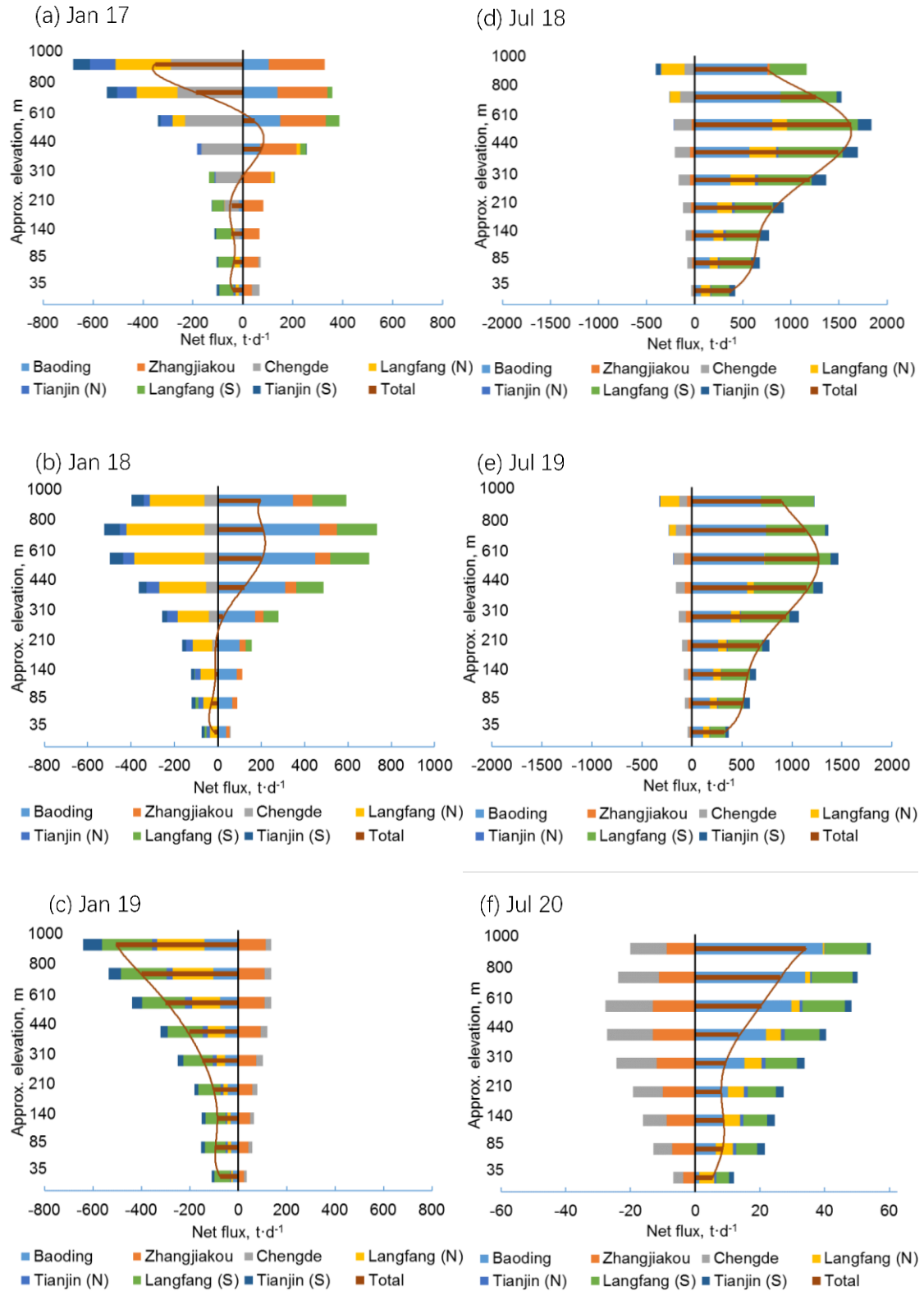


Figure R4 PM_{2.5} fluxes during heavy-pollution days in Beijing in January and July: (a) January 17th, (b) January 18th, (c) January 19th, (d) July 18th, (e) July 19th and (f) July 20th.

In addition, some precursors were also transported in the initial periods. Afterwards, the precursors will react and form particles. Could you please quantify the contributions of the particles and the precursors' transport?

Authors' reply: The transport of precursors that may transform into particles is indeed an important factor. However, only if the precursors are tracked in all the physical and chemical reactions can we quantify the contribution of the precursor's transport to the PM_{2.5}. The flux approach is not able to account for this issue, which is one of the main shortages. Nevertheless, the flux approach can capture the transport features of all primary and most of the secondary PM_{2.5}. We have some discussion on this shortage in our manuscript, and we hope that future study can combine the tracer model with the flux approach to overcome this shortage.

What's more, without the passage of large- or medium-scale meteorological system, the local mountain-plain winds emerges in North China Plain (Tang et al., 2016, Fig. 10). The alternation between the mountainous (northeast) winds that begin at 03:00 LT at night and the plain (southwest) winds that begin at 12:00 LT in the afternoon occurs. Therefore, air pollutants will transport to the northeast direction in the afternoon and then transport back during latter of half of the night. Could you please clarify the transport circulations combined with the influences of the mountain-plain winds?

Authors' reply: We thank the reviewer very much for this useful comment. In our original study, we calculated daily PM_{2.5} fluxes, so that the mountain-plain winds (which is a diurnal variation feature) is not taken the into consideration. Following the reviewer's comment, we tried to probe into the diurnal wind and flux pattern in Beijing. The simulated average diurnal wind patterns at 100 m height in January and July in Beijing are shown in Fig. R5(b). We also put the observation results from Tang et al., (2016) in Fig R5(a) as a reference. We find that the simulated wind pattern is consistent with the observation. In January, the mountain-plain winds are presented as the change in wind speed, but the wind direction does not change significantly during the whole day. In July, there is a significant wind direction shift, similar to the description of the reviewer. The mountainous wind (northeast) begins at 2:00 LT, and is taken over by the plain wind (southeast) at about 10:00 LT, and the mountainous wind is much weaker than the plain wind. A circulation of mountain-plain wind may have influence on the transport of PM_{2.5} in July.

Considering that the mountain-plain wind circulation mainly happens at the foot of the mountains, we calculated the fluxes through the boundaries between Beijing and its three neighboring cities on the south/southeast (Baoding, Langfang and Tianjin) during mountainous wind hours and the plain wind hours in July separately (Fig. R6). During the plain wind hours, all the boundaries on the southwest and southeast of Beijing have positive net fluxes, which is due to the relatively strong southerly plain winds. During the mountainous wind hours, however, there is no significant direction change of the fluxes except for the boundary of Baoding and Southern Langfang at levels below 200 m. The sign of fluxes mostly remains unchanged because the mountain-plain wind

circulation is weaker at higher levels, and the wind speed of the mountainous wind is even weaker at the southernly boundaries which has limited effect to alter the sign of the flux. Nevertheless, the magnitude of fluxes is significantly smaller than the plain wind hours, which is partly attributed to the mountain-plain wind circulation. Therefore, the summertime mountain-plain wind circulation in Beijing does not significantly alter the sign of inter-city $PM_{2.5}$ fluxes but does have considerable impact on their magnitude. We have included the discussion on the mountain-plain wind in our revised manuscripts (Page 14, Line 365-369 in the main text, and Page 12-13, Line 102-131 in SI).

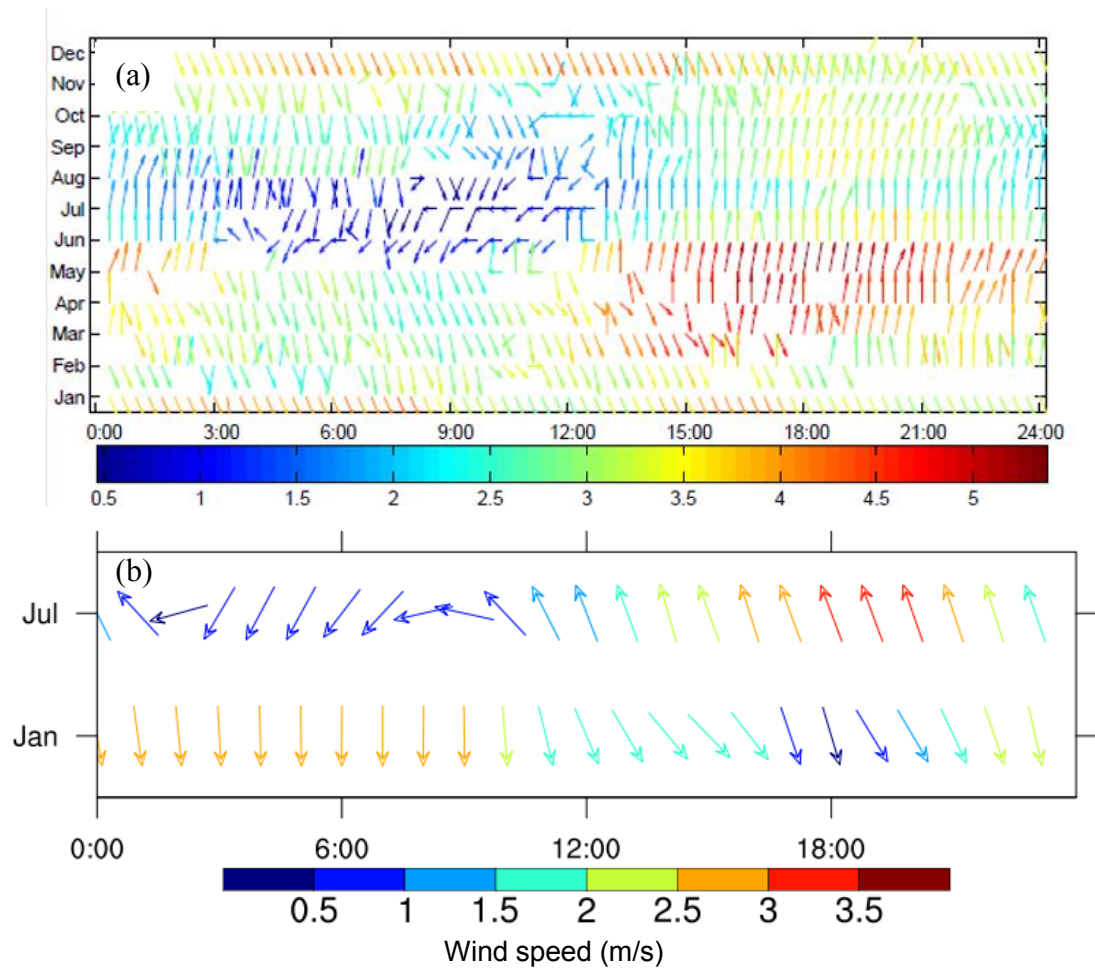


Figure R5 The observed and simulated monthly average diurnal variation of winds in Beijing in July. (a) The observation results from Tang et al. (2016). (b) The simulation results in this study.

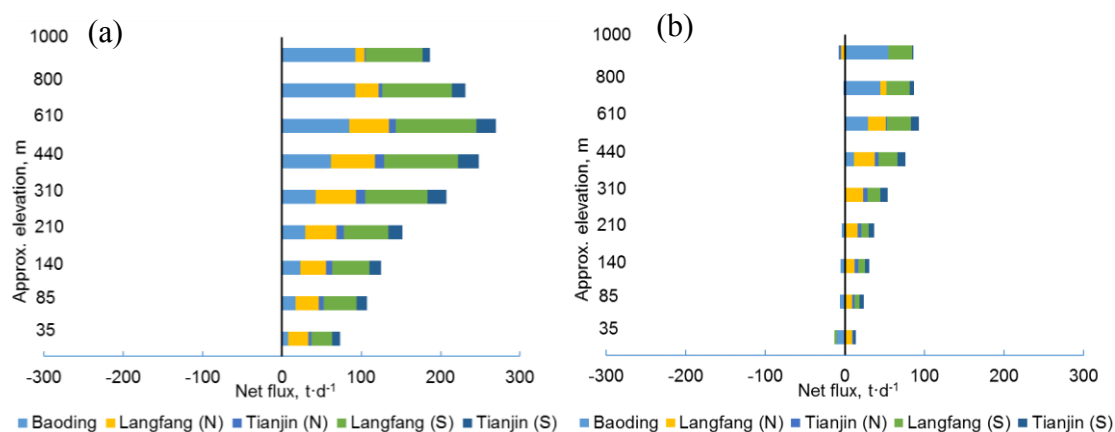


Figure R6 The transport fluxes in July between Beijing and its neighboring cities during (a) plain wind hours (11:00 – 1:00 (+1 day) LT) and (b) mountainous wind hours (2:00 – 10:00 LT)

References:

- Boylan, J. W., and Russell, A. G.: PM and light extinction model performance metrics, goals, and criteria for three-dimensional air quality models, *Atmospheric Environment*, 40, 4946-4959, 10.1016/j.atmosenv.2005.09.087, 2006.
- Emery, C., Tai, E., and Yarwood, G.: Enhanced meteorological modeling and performance evaluation for two texas episodes, Prepared for the Texas Natural Resource Conservation Commission, by ENVIRON International Corp, Novato, CA, 2001.
- Hu, J., Chen, J., Ying, Q., and Zhang, H.: One-year simulation of ozone and particulate matter in China using WRF/CMAQ modeling system, *Atmospheric Chemistry and Physics*, 16, 10333-10350, 10.5194/acp-16-10333-2016, 2016.
- Kwok, R. H. F., Baker, K. R., Napelenok, S. L., and Tonnesen, G. S.: Photochemical grid model implementation and application of VOC, NO_x, and O₃ source apportionment, *Geoscientific Model Development*, 8, 99-114, 10.5194/gmd-8-99-2015, 2015.
- Liu, J., Mauzerall, D. L., Chen, Q., Zhang, Q., Song, Y., Peng, W., Klimont, Z., Qiu, X. H., Zhang, S. Q., Hu, M., Lin, W. L., Smith, K. R., and Zhu, T.: Air pollutant emissions from Chinese households: A major and underappreciated ambient pollution source, *P. Natl. Acad. Sci. USA*, 113, 7756–7761, 2016.
- Tang, G., Zhu, X., Hu, B., Xin, J., Wang, L., Muenkel, C., Mao, G., and Wang, Y.: Impact of emission controls on air quality in Beijing during APEC 2014: lidar ceilometer observations, *Atmospheric Chemistry and Physics*, 15, 12667-12680, 10.5194/acp-15-12667-2015, 2015.
- Tang, G., Zhang, J., Zhu, X., Song, T., Muenkel, C., Hu, B., Schaefer, K., Liu, Z., Zhang, J., Wang, L., Xin, J., Suppan, P., and Wang, Y.: Mixing layer height and its implications for air pollution over Beijing, China, *Atmospheric Chemistry and Physics*, 16, 2459-2475, 10.5194/acp-16-2459-2016, 2016.
- Wang, S., Xing, J., Chatani, S., Hao, J., Klimont, Z., Cofala, J., and Amann, M.:

- Verification of anthropogenic emissions of China by satellite and ground observations, *Atmospheric Environment*, 45, 6347-6358, 10.1016/j.atmosenv.2011.08.054, 2011.
- Wang, L. T., Wei, Z., Yang, J., Zhang, Y., Zhang, F. F., Su, J., Meng, C. C., and Zhang, Q.: The 2013 severe haze over southern Hebei, China: model evaluation, source apportionment, and policy implications, *Atmospheric Chemistry and Physics*, 14, 3151-3173, 10.5194/acp-14-3151-2014, 2014.
- Wang, L., Wei, Z., Wei, W., Fu, J. S., Meng, C., and Ma, S.: Source apportionment of PM_{2.5} in top polluted cities in Hebei, China using the CMAQ model, *Atmospheric Environment*, 122, 723-736, 10.1016/j.atmosenv.2015.10.041, 2015.
- Zhao, B., Wang, S., Wang, J., Fu, J. S., Liu, T., Xu, J., Fu, X., and Hao, J.: Impact of national NO_x and SO₂ control policies on particulate matter pollution in China, *Atmospheric Environment*, 77, 453-463, 10.1016/j.atmosenv.2013.05.012, 2013.
- Zhao, B., Wu, W., Wang, S., Xing, J., Chang, X., Liou, K.-N., Jiang, J. H., Jang, C., Fu, J. S., Zhu, Y., Wang, J., and Hao, J.: A modeling study of the nonlinear response of fine particles to air pollutant emissions in the Beijing-Tianjin-Hebei region, *Atmospheric Chemistry and Physics Discussions*, 10.5194/acp-2017-428, 2017.
- Zhu, X., Tang, G., Hu, B., Wang, L., Xin, J., Zhang, J., Liu, Z., Muenkel, C., and Wang, Y.: Regional pollution and its formation mechanism over North China Plain: A case study with ceilometer observations and model simulations, *Journal of Geophysical Research-Atmospheres*, 121, 14574-14588, 10.1002/2016jd025730, 2016.

1 **Assessment of inter-city transport of particulate matter in the**
2 **Beijing-Tianjin-Hebei region**

3 Xing Chang¹, Shuxiao Wang^{1,2}, Bin Zhao³, Siyi Cai¹, and Jiming Hao^{1,2}

4 [1] State Key Joint Laboratory of Environment Simulation and Pollution Control, School of Environment,
5 Tsinghua University, Beijing 100084, China

6 [2] State Environmental Protection Key Laboratory of Sources and Control of Air Pollution Complex,
7 Beijing 100084, China

8 [3] Joint Institute for Regional Earth System Science and Engineering and Department of Atmospheric and
9 Oceanic Sciences, University of California, Los Angeles, CA 90095, USA

10
11 *Correspondence to:* Shuxiao Wang [shxwang@tsinghua.edu.cn]

12 and Bin Zhao [zhaob1206@ucla.edu]

Abstract

The regional transport of PM_{2.5} plays an important role in the air pollution of the Beijing-Tianjin-Hebei (BTH) region in China. However, previous studies on regional transport of PM_{2.5} mainly aim at province level, which is insufficient for the development of an optimal joint PM_{2.5} control strategy. In this study, we calculate PM_{2.5} inflows and outflows through the administrative boundaries of three major cities in the BTH region, i.e. Beijing, Tianjin and Shijiazhuang, using the WRF (Weather Research and Forecasting model) -CMAQ (Community Multiscale Air Quality) modelling system. The monthly average inflow fluxes indicate the major directions of PM_{2.5} transport. For Beijing, the PM_{2.5} inflow fluxes from Zhangjiakou (on the northwest) and Baoding (on the southwest) constitute 57% of the total in winter, and Langfang (on the southeast) and Baoding constitute 73% in summer. Based on the net PM_{2.5} fluxes and their vertical distributions, we find there are three major transport pathways in the BTH region: the Northwest-Southeast pathway in winter (at all levels below 1000 m), the Southeast-Northwest pathway in summer (at all levels below 1000 m), and the Southwest-Northeast pathway both in winter and in summer (mainly at 300 – 1000 m). In winter, even if surface wind speeds are low, the transport at above 300 m could still be strong. Among the three pathways, the Southwest-Northeast happens along with PM_{2.5} concentrations 30% and 55% higher than the monthly average in winter and summer, respectively. Analysis of two heavy pollution episodes in January and July in Beijing show a much stronger (8-16 times) transport than the monthly average, emphasizing the joint air pollution control of the cities located on the transport pathways, especially during heavy pollution episodes.

Key words: PM_{2.5} flux; inter-city transport; CMAQ model; Beijing-Tianjin-Hebei region

1. Introduction

The Beijing-Tianjin-Hebei (BTH) region, one of the most developed regions in China, is suffering from severe pollution of particulate matter with diameter less than 2.5 μm (PM_{2.5}). According to the monitoring data from China National Environmental Monitoring Centre (<http://www.cnemc.cn/>), the average PM_{2.5} concentrations of the BTH region in 2013, 2014 and 2015 were 106 $\mu\text{g}/\text{m}^3$, 93 $\mu\text{g}/\text{m}^3$ and 77 $\mu\text{g}/\text{m}^3$, respectively, which far exceeded the 35 $\mu\text{g}/\text{m}^3$ standard in China. The high PM_{2.5} concentrations have adverse impacts on visibility (Zhao et al., 2011b) as well as human health (Zhang et al., 2013), and thus may cause a large economic loss (Mu and Zhang, 2013). Therefore, it is urgent to reduce the PM_{2.5} concentration in the BTH region.

Emissions from one city can substantially affect the PM_{2.5} pollution in another city under particular meteorology conditions by the transport process. For example, some studies showed that emissions from outside Beijing can contribute to 28-70% of the ambient PM_{2.5} concentration in Beijing (An et al., 2007; Streets et al., 2007; BJEPB, 2015; Wang et al., 2014b). A number of approaches have been applied to evaluate the inter-city transport of PM_{2.5} and its effect on local air quality. The backward trajectory, such as the HYSPLIT model (Stein et al., 2015), is one of the most commonly used methods. This method can provide the most

49 probable transport trajectory of the air mass before it arrives at a target location; however, it cannot quantify
50 the inter-city transport of PM_{2.5}. Another commonly used method is the sensitivity analysis based on Euler 3-
51 D models, such as CMAQ (Community Multiscale Air Quality model), which is done by calculating the
52 change in concentration due to a change in emissions. This method includes the Brute Force Method (e.g.
53 Wang et al., 2015), the decoupled direct method (DDM, (Itahashi et al., 2012)), and the Response Surface
54 Model (RSM, (Zhao et al., 2015)). These methods are all based on a chemical transport model, so that the
55 physical and chemical processes can both be well considered. **However, the sensitivity of PM_{2.5} concentration**
56 **in the target city to emissions from the source city is not necessarily the same as the contribution of transport**
57 **process, because of the non-linear relationships between emissions and concentrations**(Kwok et al., 2015).

58 Based on the simulated meteorology field and air pollutant concentrations, the inter-city transport of PM_{2.5} can
59 be simply expressed by the PM_{2.5} flux through city boundaries. Compared to the preceding methods, the flux
60 approach can give direct and quantitative assessment of the transport of pollutants without a heavy calculation
61 burden. This approach has been widely applied to assess the large scale transport of air pollutants, such as
62 inter-continent transports (Berge and Jakobsen, 1998; In et al., 2007). There are also studies that evaluated the
63 pollutant transport on a regional scale (Jenner and Abiodun, 2013; Wang et al., 2009); some of which focused
64 on the BTH region (An et al., 2012; Wang et al., 2010). In those studies, the boundaries for flux calculations
65 are at the province level. However, in China, the air pollution control strategy is formulated and implemented
66 at the city level. Moreover, most previous studies regarding PM_{2.5} transports in the BTH region focused on
67 Beijing. In recent years, however, under the policy of “integrating development of BTH region”, the air quality
68 in Tianjin and the cities in Hebei Province are being increasingly emphasized. Therefore, a systematic
69 assessment of the PM_{2.5} flux at the city level in the BTH region is needed.

70 In this study, we select Beijing, Tianjin and Shijiazhuang as target cities, and calculate the inter-city PM_{2.5}
71 transport fluxes through the administrative boundaries between the target cities and the neighboring prefecture-
72 level cities, based on the WRF (Weather Research and Forecasting model) –CMAQ modeling system. The
73 PM_{2.5} transport pathway in the BTH region are identified based on the PM_{2.5} transport flux results.

75 **2. Methodology**

76 **2.1. Emission inventory**

77 A multiscale emission inventory is used in this study. For the region outside China mainland, we use the MIX
78 emission inventory (Li et al., 2017) of the year 2010. For the China mainland other than the BTH region, we
79 adopt a gridded emission inventory of 2012 developed in our previous study (Cai et al., 2017). For the BTH
80 region, we develop a bottom-up emission inventory of 2012. A unit-based approach is used for power plants,
81 iron and steel plants, and cement plants (Zhao et al., 2008). Emission factor approach is used for other sectors
82 (Fu et al., 2013; Zhao et al., 2013b). In particular, emissions in Beijing are updated from the bottom-up
83 inventory developed by Tsinghua University and Beijing Municipal Research Institute of Environmental

84 Protection (BJEPB, 2010; Zhao et al., 2011a). The emissions of major pollutants in each city are shown in
85 Table 1. Methods for the biogenic emissions, the VOC speciation and the spatial and temporal allocation of
86 emissions are consistent with our previous study (Zhao et al., 2013a). The spatial distributions of emissions
87 are shown in Fig. S1 (see the Supplementary Information (SI)).
88

89 2.2. WRF-CMAQ model configuration

90 We establish a one-way, triple nesting domain in the WRF-CMAQ model to simulate the meteorology and air
91 pollutant fields, as shown in Fig. 1. Domain 1 covers mainland China and part of East Asia and Southeast Asia
92 at a grid resolution of $36\text{ km} \times 36\text{ km}$; Domain 2 covers the eastern China at a grid resolution of $12\text{ km} \times 12$
93 km ; Domain 3 covers the BTH region at a grid resolution of $4\text{ km} \times 4\text{ km}$, which is the target area of this study.
94 The simulation periods are January and July 2012 representing the winter and summer time, respectively.

95 For the WRF (version 3.7) model, 23 sigma levels are selected for the vertical grid structure. The top layer
96 pressure is 100 mb at approximately 15 km. The National Center for Environmental Prediction (NCEP)'s Final
97 Operational Global Analysis data with a horizontal resolution of $1^\circ \times 1^\circ$ at every 6 h are used to generate the
98 first guess field. The NCEP's Automated Data Processing (ADP) data are used in the objective analysis scheme.
99 The major physics options are the Kain-Fritsch cumulus scheme, the Pleim-Xiu land surface model, the ACM2
100 planetary boundary layer (PBL) scheme, the Morrison double-moment cloud microphysics scheme, and the
101 Rapid Radiative Transfer Model (RRTM) longwave and shortwave radiation scheme. The Meteorology-
102 Chemistry Interface Processor (MCIP) version 3.3 is applied to convert the WRF output data to a format
103 required by CMAQ.

104 We use CMAQv5.0.2 to simulate the air quality field. The CMAQ model is configured with the AERO6
105 aerosol module and the CB-05 gas-phase chemical mechanism. The default profile is used to generate the
106 boundary condition of the first domain, and the simulation results of the outer domains provide the boundary
107 conditions for the inner domains. The simulation begins five days ahead of each month to minimize the impact
108 of initial condition.

109 The model predicted meteorology and $\text{PM}_{2.5}$ concentrations are compared with observation data. The results
110 are shown in the Supplementary Information (SI). The simulations agree well with observations. Most of the
111 indices are within the benchmarks suggested by Emery et al. (2001). We evaluate simulated $\text{PM}_{2.5}$
112 concentrations against observations at 5 sites located in Domain 3, i.e., Beijing, Shijiazhuang, Xianghe,
113 Xinglong and Yucheng (see Fig. 1), as shown in Table 2. The time series of simulated and observed $\text{PM}_{2.5}$
114 concentrations are shown in Fig. 2. It can be seen that the variation trends of $\text{PM}_{2.5}$ are well reproduced both
115 in January and in July for all 5 sites. The average $\text{PM}_{2.5}$ concentrations are slightly underestimated in January,
116 while the underestimation is larger in July in most sites, especially in Beijing and Xinglong. However, the
117 MFB and MFE indices in January and July for the domain all fall inside the "criteria" benchmark value
118 suggested by Boylan and Russell (2006). To understand the reason of the underestimation, it is necessary to

119 evaluate the simulation results of major components of PM_{2.5}. Given that we have no observations of PM_{2.5}
 120 components in 2012 in the BTH region, we additionally simulate the air quality in July and August in 2013,
 121 and compare it with the PM_{2.5} component observations at several sites (see details in the SI). Generally, the
 122 underestimation of total PM_{2.5} in the summer time mainly comes from the underestimation of organic carbon
 123 (OC) and sulfate. The default CMAQ tends to underestimate secondary organic aerosol to a large extent,
 124 especially in summer when photochemical reactions are active, which is a common problem of most widely
 125 used chemical transport models (Simon and Bhawe, 2012; Heald et al., 2005; Zhao et al., 2016). The lack of
 126 aqueous oxidation of SO₂ by NO₂ (Wang et al., 2016), and SO₂ oxidation at dust surface (Fu et al., 2016) may
 127 partly account for the underestimation of sulfate. The underestimation of sulfate also partly explains the
 128 overestimation of nitrate. Moreover, the biases of PM_{2.5} major components in the current study fall in a similar
 129 range with other studies in the BTH region (Wang et al., 2015; Wang et al., 2014a; Wang et al., 2011; Zhao et
 130 al., 2017; Liu et al., 2016) (See details in the SI). In conclusion, the biases of simulated meteorological field
 131 and PM_{2.5} concentrations fall in a reasonable range. The modelling results can be used for further studies.

132 2.3. PM_{2.5} flux calculation

133 The PM_{2.5} flux in this study stands for the mass of PM_{2.5} that flow through a particular vertical surface in a
 134 particular period of time. The vertical surface extends from the ground to a particular vertical level along the
 135 boundary of two regions (Fig. 3(a)). However, the model can only provide three-dimensional discrete wind
 136 field and PM_{2.5} concentration field. Therefore, the vertical surface through which the flux is calculated is
 137 discretized to several vertical grid cells, as is illustrated in Fig. 3(b) and detailed in the next paragraph. In this
 138 case, the expression of PM_{2.5} flux can be written as

$$139 \quad Flux = \sum_{i=1}^h \sum_l LH_i c \vec{v} \cdot \vec{n} \quad (1)$$

140 where l is the boundary line of two regions; h is the top layer; L is the grid width; H_i is the height between
 141 layer i and $i-1$; c is the concentration of PM_{2.5} at the vertical grid cell; \vec{v} is the wind vector, and \vec{n} is the
 142 normal vector of the vertical grid cell. The variables in the expression can be obtained from the output of the
 143 models. We choose the 9th layer above the ground (about 1000 m) as the top layer, because most of the PM_{2.5}
 144 transport between regions happens inside the boundary layer (Shi et al., 2008). Even though the transport could
 145 happen above the boundary layer, the influence of such transport on the near ground concentrations is less
 146 important because the vertical mixing above the boundary layer is weaker.

147 Beijing and Tianjin are two most important and developed megacities in the BTH region. Shijiazhuang is the
 148 capital city, and also one of the most developed and polluted cities in Hebei province. Therefore, we choose
 149 these three cities as the target cities for flux calculation. In order to accurately distinguish the transport from
 150 different adjacent cities and to understand the net PM_{2.5} inflow of a city as a whole, all the administrative
 151 boundaries between the target city and the adjacent cities are chosen as the boundary line. The boundary lines
 152 are separated to different segments by neighbor cities, and the fluxes are calculated separately for each segment.

153 The locations of the three target cities and their neighbors are shown in Fig. 1. Note that there is a small area
154 surrounded by Beijing and Tianjin that belongs to the city of Langfang, so the boundaries between Beijing and
155 Tianjin, Beijing and Langfang, and Tianjin and Langfang are each separated into two segments. To distinguish
156 them, we add the relative location of the boundary to the neighbor city's name, like "Beijing (N)" and "Beijing
157 (S)".

158 The flux varies every now and then, depending on the wind direction. The polluted air mass may flow in, affect
159 the local air quality and flow out subsequently in a short time, so that the flux may offset each other during the
160 integration. Therefore, to characterize the intensity of interactions between two regions as well as the general
161 impact of PM_{2.5} transport, three indices are chosen in regard to the flux calculation, that is the inflow flux,
162 outflow flux and net flux.

164 **3. Results and discussion**

165 **3.1. Characteristics of the inter-city PM_{2.5} transport in January**

166 The monthly inflow, outflow and net fluxes through each boundary segment of the three target cities are shown
167 in Fig. 4, from which we can get an overview of the transport in a relatively long period of time. We treat the
168 fluxes as positive if PM_{2.5} flows into the target cities, and vice versa. Therefore, the positive total net fluxes in
169 Beijing and Shijiazhuang reveal that the PM_{2.5} inflows of these two cities generally exceed the outflows, and
170 that these cities act as a "sink" of PM_{2.5}. This is possibly due to the unique terrain of Beijing and Shijiazhuang.
171 These two cities are both half-surrounded by western and northern mountains, while major emissions of PM_{2.5}
172 lie to the south and east. Consequently, pollutants are easily trapped in the bulging part of the plain if there is
173 a weak wind from the south or the east. The trapped pollutants are either scavenged by wet deposition without
174 flowing out, or diluted by strong vertical convection due to the strong northwestern wind brought by the cold
175 front and thus flow out of the boundary layer. In contrast, Tianjin behaves as a "source" of PM_{2.5} flux.
176 Furthermore, a probe into the detailed inflow, outflow and net fluxes through each boundary segment of the
177 three cities may help us understand the extent to which the cities interact with their neighbors. For Beijing, in
178 winter, the inflow fluxes mainly come from Zhangjiakou (on the northwest) and Baoding (on the southwest),
179 and the outflows go to Chengde (on the northeast) and Langfang (on the southeast) more than the others. For
180 Tianjin, Langfang (on the northwest) and Tangshan (on the northeast) contribute most of the inflow fluxes,
181 and the Bohai sea (on the southeast) and Tangshan again receive the major outflow fluxes. Shijiazhuang acts
182 differently from Beijing and Tianjin. The inflow and outflow fluxes through all the four boundary segments
183 are considerably strong, where Xingtai (on the south) and Baoding (on the northeast) contributing relatively
184 more to inflow and outflow fluxes, respectively.

185 PM_{2.5} fluxes may vary with height. We calculate the vertical distribution of net flux through each boundary
186 segment to see at what level the transport mainly occurs. The results are shown in Fig. 5 (a), (c) and (e). The
187 fluxes of each vertical layer in the CMAQ model are shown separately, and the approximate elevation of each

188 layer is marked on the left. Generally, the total flowing intensity is stronger at higher levels for all three cities,
189 while the major contributor varies with layers. If we add up the net fluxes through all boundary segments
190 (shown by the narrow bars with an envelope line), we can see that the “sink” behavior of Beijing is mainly
191 contributed by the total net fluxes at 400 to 600 m where contribution from Baoding (on the southwest) exhibits
192 a rapid increase with height. Similarly, the total net flux for Tianjin shows a peak value near 600 m where
193 Tangshan (on the northeast) receives much more outflow than it does near the ground. Total net flux for
194 Shijiazhuang shows a peak value near 400 m where Hengshui (on the east) and Xingtai (on the south) have
195 dominant contributions.

196 In order to better understand the general image of the transport characteristics in the BTH region, we display
197 the net flux results on a map, using arrows to represent the net flux direction and intensity. The result of January
198 is shown in Fig. 6(a). Bigger arrow represents larger flux, and white and black arrows denote fluxes at the
199 lower (layer 1-5 in the model, from the ground to about 310 m) and upper (layer 6-9 in the model, from about
200 310 m to about 1000 m) layers, respectively. From the map we can identify two key PM_{2.5} transport pathways
201 in the BTH region in January: the Northwest-Southeast pathway (Zhangjiakou -> Beijing -> Langfang ->
202 Tianjin -> The Bohai Sea) and the Southwest-Northeast pathway (Xingtai -> Shijiazhuang -> Baoding ->
203 Beijing -> Chengde). The former is related to the prevailing wind direction brought by winter monsoon in the
204 BTH region, and happens at both lower layers and higher layers. The latter happens mainly at higher layers.
205 According to the Ekman Spiral, wind speed is much higher at the upper level of the boundary layer (Holton
206 and Hakim, 2012), so that pollutants can travel a longer distance during their lifetime. Assuming that the
207 emission height of each city is similar, we believe that a PM_{2.5} inflow at higher altitude origins more probably
208 from a farther source. From this point of view, the PM_{2.5} flow of the Southwest-Northeast pathway at higher
209 levels may consist of a relatively long range transport. In winter time, the southwest wind field usually occurs
210 after the passage of a cold high pressure, when the wind speed is low and the sky is clear. Such air condition
211 traps less upward infrared radiation at night, which helps to enhance the air stability, or even causes
212 temperature inversion. Moreover, the southwest wind also brings moisture, leading to the formation of fog,
213 which may enhance the aqueous reaction to form more particles. Therefore, southwest wind is usually
214 accompanied by pollution. The Southwest-Northeast transport pathway should be intensely considered during
215 the winter time in the BTH region. In contrast, the northwest wind usually comes during the passage of a cold
216 high pressure, with a relatively high wind speed both at lower and higher levels bringing dry, cold and clean
217 air from the non-polluted area. The large fluxes from northwest are more likely due to the strong winds rather
218 than the high PM_{2.5} levels.

219 **3.2. Characteristics of the inter-city PM_{2.5} transport in July**

220 We conduct the same calculation in July to probe into the transport characteristics in summer. The monthly
221 average inflow, outflow and net fluxes are shown in Fig. 4. Similar to January, total net fluxes are positive
222 (more inflow than outflow) for Beijing and Shijiazhuang, and negative (more outflow than inflow) for Tianjin,

223 though the magnitude is much higher than that in January. In detail, the inflow fluxes for Beijing mainly come
224 from Langfang (on the southeast) and Baoding (on the southwest), and the outflow fluxes mainly go to
225 Chengde (on the northeast) and Zhangjiakou (on the northwest). For Tianjin, Bohai sea (on the east) and
226 Tangshan (on the northeast) contribute a large part of the inflow, and Langfang (on the northwest) and
227 Tangshan receive most of the outflow fluxes. The transport directions for Beijing and Tianjin in July are quite
228 different from those in January. However, for Shijiazhuang, all of the four directions (Shanxi, Baoding,
229 Hengshui and Xingtai) still contribute comparable amount of inflow and outflow fluxes, where inflows from
230 Xingtai (on the south) and Hengshui (on the east) are slightly larger.

231 Fig. 5 (b), (d) and (f) display the vertical distributions of monthly average net fluxes with respect to the three
232 cities in July. For Beijing, the total net fluxes are positive at all levels, which are different from those in January.
233 The major contributor, Baoding and Langfang, show different behaviors. Net flux from Baoding is nearly zero
234 near the ground, but increases rapidly with height, while the net flux from Langfang (including both Langfang
235 (N) and Langfang (S)) is significant at all levels, and is largest at medium height. These phenomena are tied
236 to the wind speed and direction at different heights in the BTH region in summer. The dominant wind direction
237 near the ground is from the southeast. Within the boundary layer, the wind will rotate clockwise and become
238 stronger at higher levels according to Ekman Spiral (Holton and Hakim, 2012). Langfang and Baoding are
239 located to the southeast and southwest of Beijing, respectively. The increase of wind speed and the rotation of
240 wind direction will constantly enhance the $PM_{2.5}$ transport from southwest, but could contribute oppositely to
241 the transport from southeast, causing a local maximum in middle layers. For Tianjin, the overall outflow
242 happens mainly at levels below 600 m, where the outflow flux mainly goes to Langfang. The inflow flux is
243 dominated by the Bohai Sea at all heights, indicating a cross-sea transport from Shandong or other areas. The
244 vertical distribution of net fluxes for Shijiazhuang is quite similar to that in January, except that Shanxi no
245 more contribute a considerable amount of inflow flux.

246 We also show the general transport characteristics in the BTH region with arrows on the map, as is shown in
247 Fig. 6(b). Compared with that in winter, the transport at lower layers becomes stronger. We can also figure out
248 two major transport pathways in BTH in July: the Southwest-Northeast pathway (Xingtai -> Shijiazhuang ->
249 Baoding -> Beijing -> Chengde), and the Southeast-Northwest pathway (Bohai -> Tianjin -> Langfang ->
250 Beijing -> Zhangjiakou, and Hengshui -> Shijiazhuang). The latter pathway, which is caused by the summer
251 monsoon, is significant at both lower and upper layers. The pathway from southwest to northeast is only
252 obvious at upper layers. Considering that in summer the vertical mixing is stronger, although the Southwest-
253 Northeast pathway is only active at higher levels, the transport may still affect the near-ground concentration
254 remarkably.

255 If we put together the transport characteristics in winter and summer, we can see that, aside from the opposite
256 transport pathways brought by the monsoon in different seasons, there is a steady transport pathway from
257 southwest to northeast in the BTH region regardless of the season. This pathway has also been found in some
258 other studies. Wu et al. (2017) analyzed the regional persistent haze events in the BTH region during 1980-

259 2013, and found that southwestern wind field at 925 hPa (~800 m) is a typical meteorology condition.
260 Backward trajectory studies by Zhao et al. (2017) also found a southerly transport pathway during pollution
261 periods in the BTH region. Therefore, the Southwest-Northeast pathway is indeed important in the BTH region.
262 To better understand how the wind and concentration affect the transport fluxes, we calculate the frequency of
263 wind directions and the corresponding wind speed and PM_{2.5} concentration, and plot them as “wind rose” plots.
264 We show the plots of Beijing in Fig. 7 as an example. The plots for the other two cities can be found in SI.
265 In January, the dominant wind directions near the ground ranges from northwest to northeast. The NNE wind
266 has the highest frequency, while the NW wind has the highest wind speed (Fig. 7(a)). The dominant northern
267 winds reflect the winter monsoon. Although the concentration coming with the northern winds are relatively
268 low because of the low emission rate on that direction(Fig. 7(b)), the high frequency and wind speed also cause
269 an overall strong transport from the northwest to the southeast. Wind directions and the corresponding
270 concentrations are quite different at the upper layers (Fig. 7(c), (d)). The prevalent northern wind remains
271 (though the dominant directions shift slightly from NNE to NW), and the frequency of southwestern winds is
272 much higher than that at lower layers. Moreover, the PM_{2.5} concentrations that come with southwestern winds
273 are much higher than the other directions. The strong emission in southern Hebei (which lies on the southwest
274 direction of Beijing), especially the elevated source may be responsible for the high concentration from the
275 southwest. Therefore, in January, the dominant northwestern winds account for the Northwest-Southeast
276 pathway at both lower layers and upper layers, while the large emissions on the southwest direction mainly
277 caused the Southwest-Northeast pathway at upper layers.
278 In July, the dominant wind directions at the lower layer are the southeastern directions, reflecting the summer
279 monsoon (Fig 7(e)), and coincidentally the highest concentrations also come along with the southeastern winds
280 (Fig 7(f)). Emissions from Tianjin, Langfang, and Tangshan may influence Beijing by the southeastern winds.
281 The emission and the wind direction both contribute to the Southeast-Northwest pathway at the lower layers.
282 The high frequency wind directions shift clockwise to the southern directions at the upper layers in July, as is
283 shown in Fig 7(g), and the southwest wind and the southeast wind are both important. Moreover, the directions
284 with high concentrations also shift to both the southwest and the southeast directions (Fig 7(h)). Therefore, in
285 July, the dominant southeastern winds and the emissions on the southeast directions caused the Southeast-
286 Northwest pathway at both the upper and the lower layers. The Southwest-Northeast pathway is a combination
287 result from the southern winds and the emissions, which is different from that in January.
288 The monthly transport characteristics could bring us inspiration on how the joint control of different cities
289 should be applied. The transport pathway at lower layers suggests that we should primarily control nearby
290 low-level emission sources, while the pathway at upper layers calls for the control over a larger region to the
291 upstream direction.
292

3.3. The daily characteristics of PM_{2.5} transport in Beijing

In addition to the monthly characteristics of PM_{2.5} transports discussed in Section 3.2, we analyzed the daily characteristics in this sector, taking Beijing as an example. Firstly, since different PM_{2.5} concentration may be caused by different meteorology condition, and may also result in different transport flux characteristics in different days, we first calculate the PM_{2.5} flux during different pollution levels (Fig. 8). We sort the daily data into 6 groups in January and 5 groups in July. The separating points are chosen to be near the 30, 55, 75, 85 and 95 percentiles in January, and the 30, 60, 80, 90 percentiles in July. The groups are denser at higher concentrations to better reveal the details around heavy pollution periods.

In January, the transport becomes stronger when the concentration is higher, but the transport flux decreases in turn when the concentration is the highest. The inflow from Baoding and outflow to Chengde, which are the indicator of the Southwest-Northeast pathway, also rise gradually, followed by a sudden decrease. In July, the situation is similar, though the decrease is less significant. Such result is consistent with Tang et al. (2015) and Zhu et al. (2016) that the Southwest-Northeast transport pathway is more significant when the pollution is still rising.

To reveal the daily characteristics comprehensively, we present the net PM_{2.5} fluxes of Beijing during two heavy-pollution episodes in January and July of 2012 as examples. In January, we choose 17th - 19th, which are the most polluted days in January (the simulated PM_{2.5} daily average concentrations all exceed 200 µg/m³). In July, we also choose the period with the highest concentration, i.e. 18th to 20th. The results are shown in Fig. 9.

The magnitude of net fluxes in January 17th and 18th (-590 t/day and 688 t/day) is much higher than the monthly average value (139 t/day). For 17th Jan, there are some weak outflows mainly to Langfang at lower levels, while stronger inflows from Baoding and Zhangjiakou occur at 300-600m. On 18th Jan, fluxes at lower level remain relatively small though the inflow and outflow directions reverse. However, strong inputs from Baoding and Langfang at above 300 m become significantly strong. It can be seen that although the fluxes near the ground are small, the inflow transport can be quite strong at levels above 300 m. Coincidentally, the elevation of the mountains in the northwest of Beijing are commonly higher than 300 m, making it harder for the inflowing PM_{2.5} to flow out. The large amount of PM_{2.5} inflows can only be efficiently blown out to the northeast direction (Chengde, Langfang (N) and Tianjin (N)). These results are consistent with Jiang et al. (2015), who also found a strong southerly input at a high level during a haze episode in winter.

However, in 19th January when the concentration reaches the peak, the inflow transport becomes weaker than the previous days, especially for the southwest inflow. The PM_{2.5} experienced a significant inflow from the southwest followed by an accumulation period with little inflow. Therefore, the Southwest-Northeast pathway is of great importance during the first days of this heavy pollution period.

For the day with the highest concentration in July (July 20th), the vertical distribution does not show much difference from the average of July (Fig. 5 (f)), except for the magnitude. The fluxes are about 1/5 of the monthly average, or less than 1/10 of that in the heavy-pollution period in January. This result suggests that

329 the heavy pollution in Beijing in 20th July is not dominated by the inter-city transport during that very day.
330 However, situations are totally different on 18th and 19th July (Fig. 7 (d,e)), the days when the simulated PM_{2.5}
331 concentration reaches a high level but is still rising in this pollution episode. The magnitude of fluxes is about
332 6 times larger than the monthly average, or some 30 times larger than that on 20th July. More importantly, the
333 outflow flux is much smaller than the inflow flux contributed mainly by Baoding and Langfang, which
334 correspond to the Southwest-Northeast and Southeast-Northwest pathways respectively. Therefore, we can
335 draw an image about how the PM_{2.5} transport affects the air quality in Beijing during this pollution episode.
336 On 18th July, the PM_{2.5} start to flow into Beijing through the Southeast-Northwest and Southwest-Northeast
337 pathways with a very strong flux, but very few of them flow out, causing the accumulative increase of PM_{2.5}
338 concentration. On 20th July, the wind field become stable and the transport weakened, but the PM_{2.5} that have
339 flowed in before accumulate to form the heavy pollution. This result indicates that both the Southeast-
340 Northwest and the Southwest-Northeast pathway are important for Beijing during this polluted period, and the
341 emission from outside Beijing should be controlled at least 2 days in advance to reduce the peak concentration.
342 From the discussions above, we can see that PM_{2.5} transport plays an important role in the heavy-pollution
343 periods in Beijing. We further analyze the PM_{2.5} flux data of the three cities day by day, and try to identify the
344 presence of transport pathway for each day in Beijing, based on whether the inflow flux from a certain direction
345 is significantly larger than the others. Finally, 8 days in January and 4 days in July are subject to the transport
346 of Southwest-Northeast pathway, 22 days in January are subject to the transport of Northwest-Southeast
347 pathway, and 8 days in July are subject to the transport of the Southeast-Northwest pathway. In July, there are
348 other 8 days that are subject to both the Southeast-Northwest pathway and the Southwest-Northeast pathway
349 (“SE-NW + SW-NE” for short). Moreover, some days do not show a clear transport direction, which are
350 referred to as “unclassifiable days”. We calculate the average simulated concentration for each transport
351 pathway. The results are shown in Table 3.

352 The days with Southwest-Northeast pathway show the highest PM_{2.5} average concentrations among all days
353 in both January and July. Therefore, the Southwest-Northeast pathway should be the focus of control strategies.
354 In contrast, the Northwest-Southeast pathway tends to happen along with the lowest concentrations in both
355 seasons. Note that in January, the day with the highest concentration (January 19th) is coincidentally identified
356 as the Northwest-Southeast pathway. That day is on the eve of the rapid clearing by the northwest wind (Fig.
357 2(a)). While the cold front is passing, the heavy polluted air mass is forced to move from northwest to southeast,
358 which cause a significant transport. However, since the pollution brought by such transport usually happen
359 with a strong cold front, the PM_{2.5} concentration will soon become very low (Jia et al., 2008). If we exclude
360 January 19th from the Northwest-Southeast pathway days, the average concentration will be only 48.5 $\mu\text{g}/\text{m}^3$.
361 In July, the Southeast-Northwest pathway and the Southwest-Northeast pathway happen simultaneously in 8
362 days. The average concentration is 47.4 $\mu\text{g}/\text{m}^3$, the second highest in July, which further emphasizes the
363 importance of the transport from the southwest. In summary, the Southwest-Northeast pathway should be taken
364 great consideration both in January and July, followed by the Southeast-Northwest pathway in July.

Besides the daily variability of $PM_{2.5}$ transport, we also analyzed the diurnal variability brought by the “mountain – plain wind cycle” in summer times in Beijing (Tang et al., 2016). However, because the average plain wind is much stronger than the mountainous wind which is only obvious below 200 m, the fluxes brought by the mountainous wind is much weaker than that by plain wind (Fig. S6). The diurnal variation of winds does not have a significant influence on the direction of the transport fluxes.

4. Conclusions

By calculating $PM_{2.5}$ inflow and outflow fluxes through the boundaries between each two prefecture-level cities, this study has shown the major $PM_{2.5}$ input and output directions in winter and summer for Beijing, Tianjin, and Shijiazhuang. For Beijing, the inflow fluxes mainly come from northwest and southwest in winter, and southeast and southwest in summer. For Tianjin, the inflow fluxes are mostly from northwest and northeast in winter, and east and northeast in summer. In Shijiazhuang, however, the four neighboring regions contribute comparable amount of inflow fluxes both in winter and summer.

By analyzing the net $PM_{2.5}$ fluxes and their vertical distribution, we identify several major transport pathways and the height they occur: the Northwest-Southeast pathway in winter (at all levels below 1000 m, but stronger at levels above 300 m), the Southeast-Northwest pathway in summer (at all levels below 1000 m), and the Southwest-Northeast pathway both in winter and in summer (at levels between 300 m and 1000 m). Although the third pathway does not happen as frequently as the other two in corresponding seasons, it is accompanied by quite high $PM_{2.5}$ concentrations in both seasons. Additionally, the relatively large transport height of this pathway suggests the importance of the long-range transport of $PM_{2.5}$ on air quality. Specially, in winter, even if the wind speed near the ground is low, which we often refer to as “steady” conditions, the transport above 300 m, which is primarily associated with long-range transport, could still be strong. These findings suggest that the joint control for cities on the Southwest-Northeast pathway should be emphasized both in winter and summer.

By analyzing daily transport fluxes in Beijing, we also find that the flux during the days with higher $PM_{2.5}$ concentration is generally higher, but the flux during the top 10% polluted days is smaller. The flux during heavy-pollution episodes is stronger than the monthly average for the two polluted periods investigated in this study. In the heavy pollution episode in summer, $PM_{2.5}$ flows into Beijing and accumulates for two days, leading to a heavy pollution. Therefore, mitigating emissions from a larger area may be essential for the control of ambient $PM_{2.5}$ in Beijing. Moreover, it appears important to control the upstream sources several days ahead to mitigate the $PM_{2.5}$ accumulations, rather than only taking actions when the pollution is already heavy. However, we must note that the two episodes we studied may not represent the general characteristics of heavy-pollution episodes, which requires a more systematic analysis in the future.

The current study has several limitations. First, we only quantify the transport of $PM_{2.5}$ at the boundary of the city, which is not the only way by which transport process may influence the $PM_{2.5}$ concentration in the target

city. Other processes include the inter-city transport of gaseous precursors that remain in gaseous phase at the boundary but may convert to secondary PM_{2.5} in the target city. Secondly, the PM_{2.5} transported through the outer boundary is a mixture of different sources that does not only from the neighbor city itself. Although we have obtained a general transport feature in the BTH region which can facilitate a qualitative understanding of where the fluxes are mainly from, the flux approach cannot quantitatively evaluate the contribution from each city in the upstream areas. If we want to overcome these disadvantages, a life-time tracing during the emission, transportation, reaction and deposition processes of PM_{2.5} and its gaseous precursors is needed. Therefore, future studies may combine the flux calculation with the tagging models to overcome these defects. Despite these limitations, the flux approach has indeed proved to be a powerful tool to visually assess the inter-city transport of pollutants.

Acknowledgments

We hereby express our gratitude to Yangjun Wang from Shanghai University, Jia Xing from Tsinghua University and Jiandong Wang from Max Planck Institute who helped us set up the modelling system and gave us useful suggestions.

This research has been supported by National Science Foundation of China (21625701 & 21521064). The simulations were completed on the “Explorer 100” cluster system of Tsinghua National Laboratory for Information Science and Technology.

References

- An, J., Li, J., Zhang, W., Chen, Y., Qu, Y., and Xiang, W.: Simulation of transboundary transport fluxes of air pollutants among Beijing, Tianjin, and Hebei Province of China, *Acta Scientiae Circumstantiae*, 32, 2684-2692, 2012.
- An, X., Zhu, T., Wang, Z., Li, C., and Wang, Y.: A modeling analysis of a heavy air pollution episode occurred in Beijing, *Atmospheric Chemistry and Physics*, 7, 3103-3114, 2007.
- Berge, E., and Jakobsen, H. A.: A regional scale multi-layer model for the calculation of long-term transport and deposition of air pollution in Europe, *Tellus Series B-Chemical and Physical Meteorology*, 50, 205-223, 10.1034/j.1600-0889.1998.t01-2-00001.x, 1998.
- BJEPB: Preliminary study of the atmospheric environment protection strategy in The 12th Five-year Plan, Beijing, China, 44-56, 2010.
- BJEPB: Beijing Environmental Statement 2014, in, <http://www.bjepb.gov.cn/bjepb/resource/cms/2015/04/2015041609380279715.pdf>, 2015.
- Boylan, J. W., and Russell, A. G.: PM and light extinction model performance metrics, goals, and criteria for three-dimensional air quality models, *Atmospheric Environment*, 40, 4946-

434 4959, 10.1016/j.atmosenv.2005.09.087, 2006.

435 Cai, S., Wang, Y., Zhao, B., Wang, S., Chang, X., and Hao, J.: The impact of the "Air Pollution
436 Prevention and Control Action Plan" on PM_{2.5} concentrations in Jing-Jin-Ji region during
437 2012-2020, *The Science of the total environment*, 580, 197-209,
438 10.1016/j.scitotenv.2016.11.188, 2017.

439 Emery, C., Tai, E., and Yarwood, G.: Enhanced meteorological modeling and performance
440 evaluation for two Texas episodes, Prepared for the Texas Natural Resource Conservation
441 Commission, by ENVIRON International Corp, Novato, CA, 2001.

442 Fu, X., Wang, S., Zhao, B., Xing, J., Cheng, Z., Liu, H., and Hao, J.: Emission inventory of
443 primary pollutants and chemical speciation in 2010 for the Yangtze River Delta region, China,
444 *Atmospheric Environment*, 70, 39-50, 10.1016/j.atmosenv.2012.12.034, 2013.

445 Fu, X., Wang, S., Chang, X., Cai, S., Xing, J., and Hao, J.: Modeling analysis of secondary
446 inorganic aerosols over China: pollution characteristics, and meteorological and dust impacts,
447 *Scientific Reports*, 6, 10.1038/srep35992, 2016.

448 Heald, C. L., Jacob, D. J., Park, R. J., Russell, L. M., Huebert, B. J., Seinfeld, J. H., Liao, H.,
449 and Weber, R. J.: A large organic aerosol source in the free troposphere missing from current
450 models, *Geophysical Research Letters*, 32, 10.1029/2005gl023831, 2005.

451 Holton, J. R., and Hakim, G. J.: An introduction to dynamic meteorology, 5th ed., Elsevier,
452 MA, USA, 532 pp., 2012.

453 In, H.-J., Byun, D. W., Park, R. J., Moon, N.-K., Kim, S., and Zhong, S.: Impact of
454 transboundary transport of carbonaceous aerosols on the regional air quality in the United
455 States: A case study of the South American wildland fire of May 1998, *Journal of Geophysical
456 Research-Atmospheres*, 112, 10.1029/2006jd007544, 2007.

457 Itahashi, S., Uno, I., and Kim, S.: Source Contributions of Sulfate Aerosol over East Asia
458 Estimated by CMAQ-DDM, *Environmental Science & Technology*, 46, 6733-6741,
459 10.1021/es300887w, 2012.

460 Jenner, S. L., and Abiodun, B. J.: The transport of atmospheric sulfur over Cape Town,
461 *Atmospheric Environment*, 79, 248-260, 10.1016/j.atmosenv.2013.06.010, 2013.

462 Jia, Y., Rahn, K. A., He, K., Wen, T., and Wang, Y.: A novel technique for quantifying the
463 regional component of urban aerosol solely from its sawtooth cycles, *Journal of Geophysical
464 Research-Atmospheres*, 113, 10.1029/2008jd010389, 2008.

465 Jiang, C., Wang, H., Zhao, T., and Che, H.: Modeling study of PM_{2.5} pollutant transport across
466 cities in China's Jing-Jin-Ji region during a severe haze episode in December 2013,
467 *Atmospheric Chemistry and Physics*, 5803-5814, 10.5194/acp-15-5803-2015, 2015.

468 Kwok, R. H. F., Baker, K. R., Napelenok, S. L., and Tonnesen, G. S.: Photochemical grid model
469 implementation and application of VOC, NO_x, and O₃ source apportionment, *Geoscientific*

470 Model Development, 8, 99-114, 10.5194/gmd-8-99-2015, 2015.

471 Li, M., Zhang, Q., Kurokawa, J.-i., Woo, J.-H., He, K., Lu, Z., Ohara, T., Song, Y., Streets, D.
472 G., Carmichael, G. R., Cheng, Y., Hong, C., Huo, H., Jiang, X., Kang, S., Liu, F., Su, H., and
473 Zheng, B.: MIX: a mosaic Asian anthropogenic emission inventory under the international
474 collaboration framework of the MICS-Asia and HTAP, *Atmospheric Chemistry and Physics*,
475 17, 935-963, 10.5194/acp-17-935-2017, 2017.

476 Liu, J., Mauzerall, D. L., Chen, Q., Zhang, Q., Song, Y., Peng, W., Klimont, Z., Qiu, X., Zhang,
477 S., Hu, M., Lin, W., Smith, K. R., and Zhu, T.: Air pollutant emissions from Chinese
478 households: A major and underappreciated ambient pollution source, *Proceedings of the*
479 *National Academy of Sciences of the United States of America*, 113, 7756-7761,
480 10.1073/pnas.1604537113, 2016.

481 Mu, Q., and Zhang, S.-q.: An evaluation of the economic loss due to the heavy haze during
482 January 2013 in China, *China Environmental Science*, 33, 2087-2094, 2013.

483 Shi, C., Yao, Y., Zhang, P., and Qiu, M.: Transport Trajectory Classifying of PM₁₀ in Hefei,
484 *Plateau Meteorology*, 27, 1383-1391, 2008.

485 Simon, H., and Bhave, P. V.: Simulating the Degree of Oxidation in Atmospheric Organic
486 Particles, *Environmental Science & Technology*, 46, 331-339, 10.1021/es202361w, 2012.

487 Stein, A. F., Draxler, R. R., Rolph, G. D., Stunder, B. J. B., Cohen, M. D., and Ngan, F.:
488 NOAA'S HYSPLIT ATMOSPHERIC TRANSPORT AND DISPERSION MODELING
489 SYSTEM, *Bulletin of the American Meteorological Society*, 96, 2059-2077, 10.1175/bams-d-
490 14-00110.1, 2015.

491 Streets, D. G., Fu, J. S., Jang, C. J., Hao, J., He, K., Tang, X., Zhang, Y., Wang, Z., Li, Z.,
492 Zhang, Q., Wang, L., Wang, B., and Yu, C.: Air quality during the 2008 Beijing Olympic
493 Games, *Atmospheric Environment*, 41, 480-492, 10.1016/j.atmosenv.2006.08.046, 2007.

494 Tang, G., Zhu, X., Hu, B., Xin, J., Wang, L., Muenkel, C., Mao, G., and Wang, Y.: Impact of
495 emission controls on air quality in Beijing during APEC 2014: lidar ceilometer observations,
496 *Atmospheric Chemistry and Physics*, 15, 12667-12680, 10.5194/acp-15-12667-2015, 2015.

497 Tang, G., Zhang, J., Zhu, X., Song, T., Muenkel, C., Hu, B., Schaefer, K., Liu, Z., Zhang, J.,
498 Wang, L., Xin, J., Suppan, P., and Wang, Y.: Mixing layer height and its implications for air
499 pollution over Beijing, China, *Atmospheric Chemistry and Physics*, 16, 2459-2475,
500 10.5194/acp-16-2459-2016, 2016.

501 Wang, G., Zhang, R., Gomez, M. E., Yang, L., Zamora, M. L., Hu, M., Lin, Y., Peng, J., Guo,
502 S., Meng, J., Li, J., Cheng, C., Hu, T., Ren, Y., Wang, Y., Gao, J., Cao, J., An, Z., Zhou, W., Li,
503 G., Wang, J., Tian, P., Marrero-Ortiz, W., Secret, J., Du, Z., Zheng, J., Shang, D., Zeng, L.,
504 Shao, M., Wang, W., Huang, Y., Wang, Y., Zhu, Y., Li, Y., Hu, J., Pan, B., Cai, L., Cheng, Y.,
505 Ji, Y., Zhang, F., Rosenfeld, D., Liss, P. S., Duce, R. A., Kolb, C. E., and Molina, M. J.:

506 Persistent sulfate formation from London Fog to Chinese haze, *Proceedings of the National*
507 *Academy of Sciences of the United States of America*, 113, 13630-13635,
508 10.1073/pnas.1616540113, 2016.

509 Wang, K., Zhang, Y., Jang, C., Phillips, S., and Wang, B.: Modeling intercontinental air
510 pollution transport over the trans-Pacific region in 2001 using the Community Multiscale Air
511 Quality modeling system, *Journal of Geophysical Research-Atmospheres*, 114,
512 10.1029/2008jd010807, 2009.

513 Wang, L., Wei, Z., Wei, W., Fu, J. S., Meng, C., and Ma, S.: Source apportionment of PM_{2.5}
514 in top polluted cities in Hebei, China using the CMAQ model, *Atmospheric Environment*, 122,
515 723-736, 10.1016/j.atmosenv.2015.10.041, 2015.

516 Wang, L. T., Wei, Z., Yang, J., Zhang, Y., Zhang, F. F., Su, J., Meng, C. C., and Zhang, Q.: The
517 2013 severe haze over southern Hebei, China: model evaluation, source apportionment, and
518 policy implications, *Atmospheric Chemistry and Physics*, 14, 3151-3173, 10.5194/acp-14-
519 3151-2014, 2014a.

520 Wang, S., Xing, J., Chatani, S., Hao, J., Klimont, Z., Cofala, J., and Amann, M.: Verification
521 of anthropogenic emissions of China by satellite and ground observations, *Atmospheric*
522 *Environment*, 45, 6347-6358, 10.1016/j.atmosenv.2011.08.054, 2011.

523 Wang, W., Wang, Z., Wu, Q., Gbaguidi, A., Zhang, W., Yan, P., and Yang, T.: Variation of PM₁₀
524 Flux and Scenario Analysis before and after the Olympic Opening Ceremony in Beijing,
525 *Climatic and Environmental Research*, 15, 652-661, 2010.

526 Wang, Z., Li, J., Wang, Z., Yang, W., Tang, X., Ge, B., Yan, P., Zhu, L., Chen, X., Chen, H.,
527 Wand, W., Li, J., Liu, B., Wang, X., Wand, W., Zhao, Y., Lu, N., and Su, D.: Modeling study
528 of regional severe hazes over mid-eastern China in January 2013 and its implications on
529 pollution prevention and control, *Science China-Earth Sciences*, 57, 3-13, 10.1007/s11430-
530 013-4793-0, 2014b.

531 Wu, P., Ding, Y., and Liu, Y.: Atmospheric circulation and dynamic mechanism for persistent
532 haze events in the Beijing-Tianjin-Hebei region, *Advances in Atmospheric Sciences*, 34, 429-
533 440, 10.1007/s00376-016-6158-z, 2017.

534 Zhang, Y., Ma, G., Yu, F., and Cao, D.: Health damage assessment due to PM_(2.5) exposure
535 during haze pollution events in Beijing-Tianjin-Hebei region in January 2013, *National*
536 *Medical Journal of China*, 93, 2707-2710, 2013.

537 Zhao, B., Xu, J., and Hao, J.: Impact of energy structure adjustment on air quality: a case study
538 in Beijing, China, *Frontiers of Environmental Science & Engineering in China*, 5, 378-390,
539 10.1007/s11783-011-0357-8, 2011a.

540 Zhao, B., Wang, S., Wang, J., Fu, J. S., Liu, T., Xu, J., Fu, X., and Hao, J.: Impact of national
541 NO_x and SO₂ control policies on particulate matter pollution in China, *Atmospheric*

542 Environment, 77, 453-463, 10.1016/j.atmosenv.2013.05.012, 2013a.

543 Zhao, B., Wang, S. X., Liu, H., Xu, J. Y., Fu, K., Klimont, Z., Hao, J. M., He, K. B., Cofala, J.,
544 and Amann, M.: NO_x emissions in China: historical trends and future perspectives,
545 Atmospheric Chemistry and Physics, 13, 9869-9897, 10.5194/acp-13-9869-2013, 2013b.

546 Zhao, B., Wang, S. X., Xing, J., Fu, K., Fu, J. S., Jang, C., Zhu, Y., Dong, X. Y., Gao, Y., Wu,
547 W. J., Wang, J. D., and Hao, J. M.: Assessing the nonlinear response of fine particles to
548 precursor emissions: development and application of an extended response surface modeling
549 technique v1.0, Geoscientific Model Development, 8, 115-128, 10.5194/gmd-8-115-2015,
550 2015.

551 Zhao, B., Wang, S., Donahue, N. M., Jathar, S. H., Huang, X., Wu, W., Hao, J., and Robinson,
552 A. L.: Quantifying the effect of organic aerosol aging and intermediate-volatility emissions on
553 regional-scale aerosol pollution in China, Scientific Reports, 6, 10.1038/srep28815, 2016.

554 Zhao, B., Wu, W., Wang, S., Xing, J., Chang, X., Liou, K.-N., Jiang, J. H., Jang, C., Fu, J. S.,
555 Zhu, Y., Wang, J., and Hao, J.: A modeling study of the nonlinear response of fine particles to
556 air pollutant emissions in the Beijing-Tianjin-Hebei region, Atmospheric Chemistry and
557 Physics Discussions, 10.5194/acp-2017-428, 2017.

558 Zhao, P., Zhang, X., Xu, X., and Zhao, X.: Long-term visibility trends and characteristics in
559 the region of Beijing, Tianjin, and Hebei, China, Atmospheric Research, 101, 711-718,
560 10.1016/j.atmosres.2011.04.019, 2011b.

561 Zhao, Y., Wang, S., Duan, L., Lei, Y., Cao, P., and Hao, J.: Primary air pollutant emissions of
562 coal-fired power plants in China: Current status and future prediction, Atmospheric
563 Environment, 42, 8442-8452, 10.1016/j.atmosenv.2008.08.021, 2008.

564 Zhu, X., Tang, G., Hu, B., Wang, L., Xin, J., Zhang, J., Liu, Z., Muenkel, C., and Wang, Y.:
565 Regional pollution and its formation mechanism over North China Plain: A case study with
566 ceilometer observations and model simulations, Journal of Geophysical Research-
567 Atmospheres, 121, 14574-14588, 10.1002/2016jd025730, 2016.

568

569 **Table 3 Summary of the emissions of major pollutants in Beijing, Tianjin and 11 prefecture-level cities**
 570 **in Hebei in 2012**

Emissions (kt/year)	NO _x	SO ₂	PM _{2.5}	PM ₁₀	BC	OC	NMVOCs	NH ₃ ^a
Beijing	202	120	75	177	9	9	381	52
Tianjin	392	287	113	151	17	26	287	45
Hebei	1620	1079	875	1172	141	221	1346	628
Shijiazhuang	270	198	149	203	23	33	230	87
Chengde	84	45	37	49	6	10	56	34
Zhangjiakou	112	52	41	54	7	11	56	35
Qinhuangdao	71	39	30	40	5	8	51	22
Tangshan	266	145	100	135	15	24	181	68
Langfang	79	71	63	86	10	14	100	35
Baoding	158	123	118	155	20	33	202	89
Cangzhou	149	121	109	148	17	25	164	67
Hengshui	79	66	62	84	10	15	92	50
Xingtai	140	105	77	102	13	21	113	60
Handan	213	115	89	117	15	26	148	82

571

572

Table 2 Comparison of the simulated and observed PM_{2.5} concentrations at five sites.

Indices	Mean OBS	Mean SIM ^a	NMB	NME	MFB	MFE	
Unit	μg·m ⁻³	μg·m ⁻³	%	%	%	%	
January, 2012	Beijing	86.0	65.2	-24.2	32.2		
	Shijiazhuang	193.9	170.8	-11.9	45.3		
	Xianghe	132.3	85.6	-35.3	44.5	-19.6	19.6
	Xinglong	39.4	38.6	-2.0	42.7		
	Yucheng	140.9	124.1	-11.9	31.2		
July, 2012	Beijing	68.2	35.6	-47.8	49.5		
	Shijiazhuang	70.3	79.8	+13.6	37.6		
	Xianghe	61.3	47.2	-23.0	35.6	-35.1	40.2
	Xinglong	48.9	24.6	-49.6	53.8		
	Yucheng	77.3	55.2	-28.6	39.6		
“Criteria” benchmark ^b	-	-	-	-	≤±60	≤75	
“Goal” benchmark ^b	-	-	-	-	≤±30	≤50	

573

a. Average of the days only when observations are available.

574

b. Benchmarks are suggested by Boylan and Russell (2006).

575

576 **Table 3 The mean and maximum simulated PM_{2.5} concentrations in Beijing for all days in January and**
 577 **July and for the days that belong to particular transport pathways.**

Month	Pathway type	Days	Mean PM _{2.5} conc in Beijing, µg/m ³	Max PM _{2.5} conc in Beijing, µg/m ³
Jan	All days	31	65.2	270.7
	Southwest-Northeast	8	85.1	211.5
	Northwest-Southeast	22	58.6	270.7
	Unclassifiable day(s)	1	53.0	53.0
Jul	All days	31	35.0	94.4
	Southwest-Northeast	4	54.2	94.4
	Northwest-Southeast	5	15.4	30.9
	Southeast-Northwest	8	29.4	53.2
	SW-NE + SE-NW	8	47.4	71.0
	Unclassifiable day(s)	9	29.3	79.7

578

579 **Figure Captions**

580 **Figure 1. The simulation domains used in this study (left) and the map of the Beijing-Tianjin-Hebei**

581 **region (right). The highlighted cities are the target cities for flux calculation. The red circles show the**

582 **sites with PM_{2.5} observations. The two sites with green circles have observations of PM_{2.5} chemical**

583 **components in 2013.**

584 **Figure 2. Time series of the simulated and observed PM_{2.5} concentrations in (a) Beijing, (b) Shijiazhuang,**

585 **(c) Xianghe, (d) Xinglong, and (e) Yucheng.**

586 **Figure 3. An example of the vertical surface for flux calculation (a) before discretization, and (b) after**

587 **discretization.**

588 **Figure 4. The inflow, outflow and net fluxes in January and July for (a) Beijing, (b) Tianjin, and (c)**

589 **Shijiazhuang.**

590 **Figure 5. Vertical distribution of net fluxes in January (left) and July (right) for (a-b) Beijing, (c-d)**

591 **Tianjin, and (e-f) Shijiazhuang**

592 **Figure 6. The transport fluxes through each boundary segment of the three target cities in January (a)**

593 **and July (b). The size of the arrows represents the amount of the fluxes, while white and black arrows**

594 **denote fluxes at the lower (layer 1-5 in the model, from the ground to about 310 m) and upper (layer 6-**

595 **9 in the model, from about 310 m to about 1000 m) layers, respectively.**

596 **Figure 7. The wind rose plots showing the frequency of wind speed (a, c, e, g) and PM_{2.5} concentration**

597 **(b, d, f, h) at different wind directions for Beijing. The ground level and the 7th level (about 450-600 m)**

598 **in the model are chosen as the representation of lower levels and upper levels. The percentages denote**

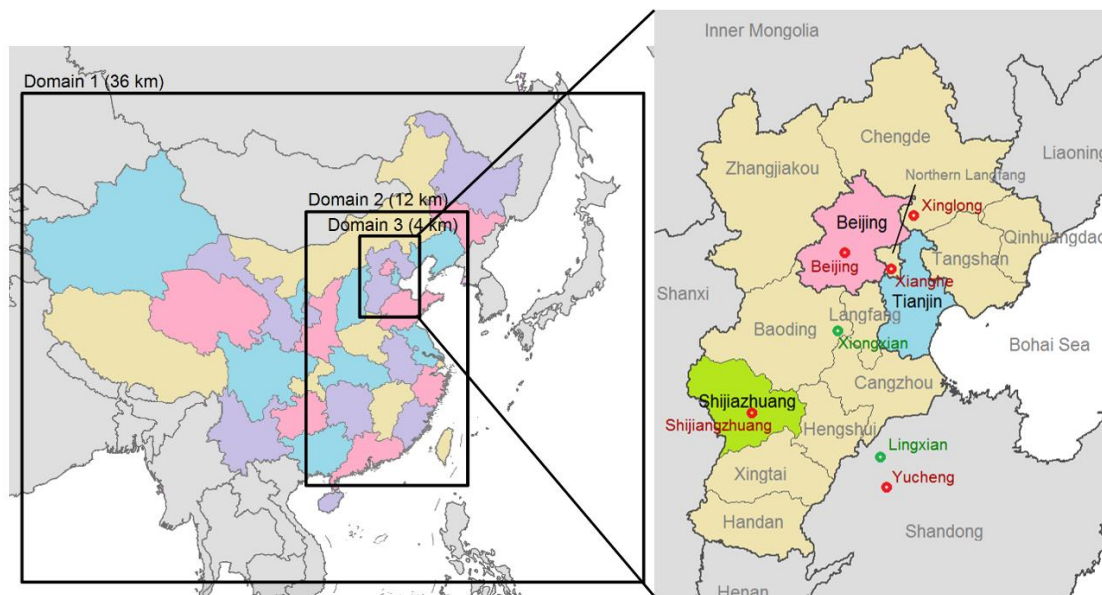
599 **the frequency.**

600 **Figure 8. PM_{2.5} average flux in different pollution degrees in (a) January and (b) July.**

601 **Figure 9. PM_{2.5} fluxes during heavy-pollution days in Beijing in January and July: (a) January 17th, (b)**

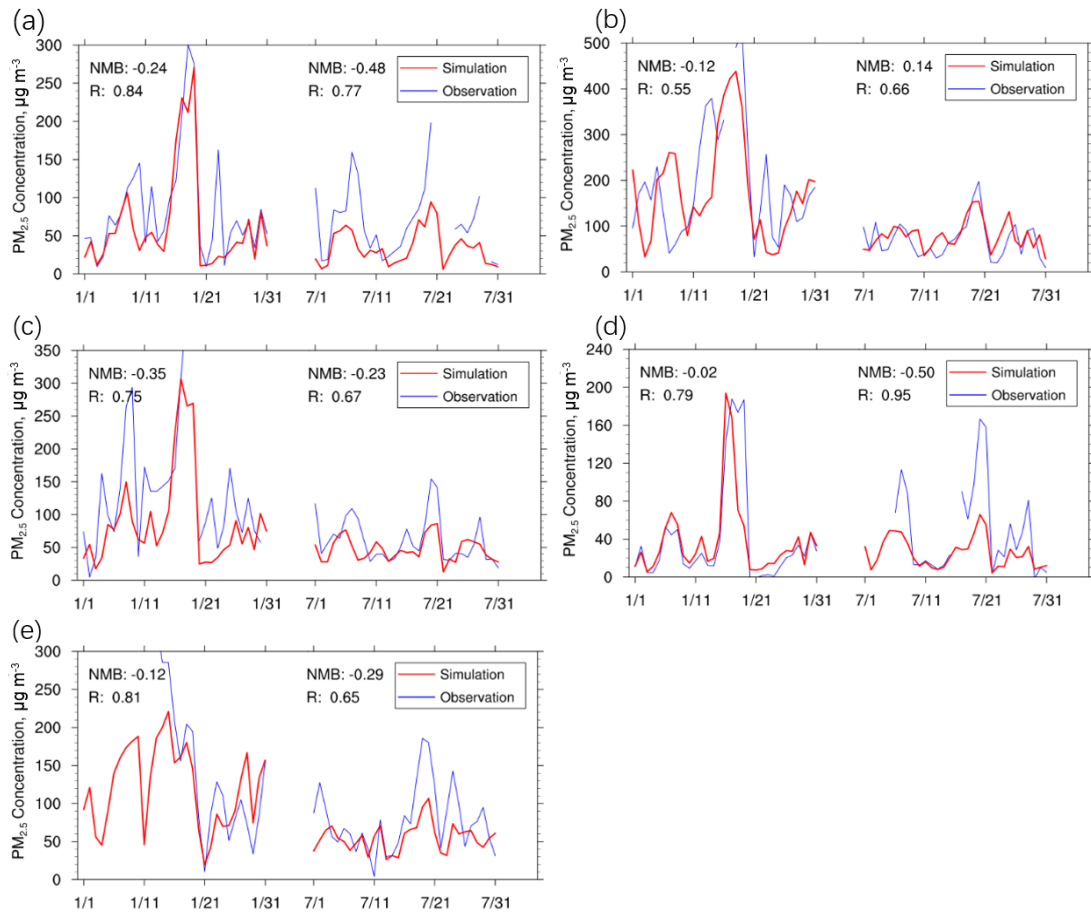
602 **January 18th, (c) January 19th, (d) July 18th, (e) July 19th and (f) July 20th..**

603



604
 605
 606
 607
 608
 609

Figure 1 The simulation domains used in this study (left) and the map of the Beijing-Tianjin-Hebei region (right). The highlighted cities are the target cities for flux calculation. The red circles show the sites with PM_{2.5} observations. The two sites with green circles have observations of PM_{2.5} chemical components in 2013.



610

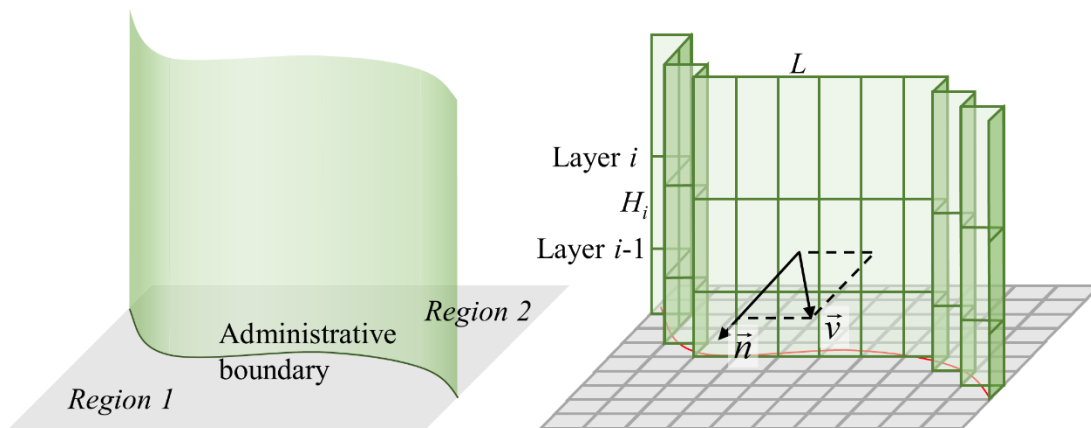
611

Figure 2 Time series of the simulated and observed PM_{2.5} concentrations in (a) Beijing, (b) Shijiazhuang,

612

(c) Xianghe, (d) Xinglong, and (e) Yucheng

613



614

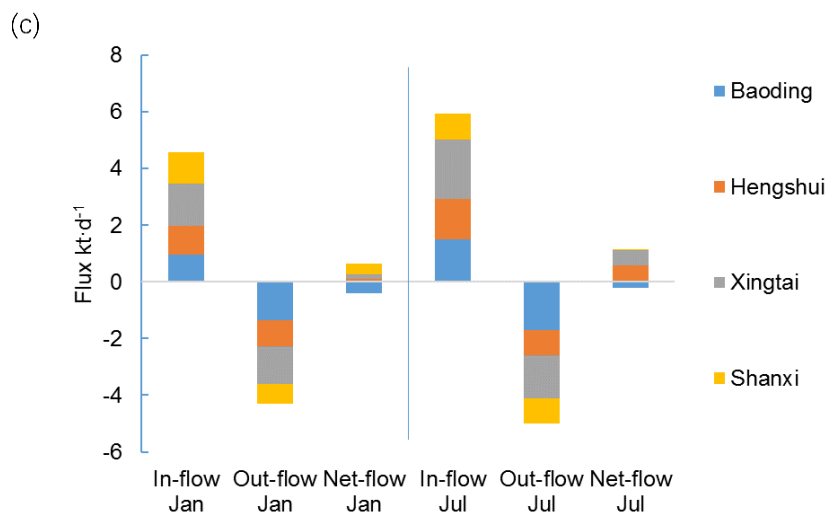
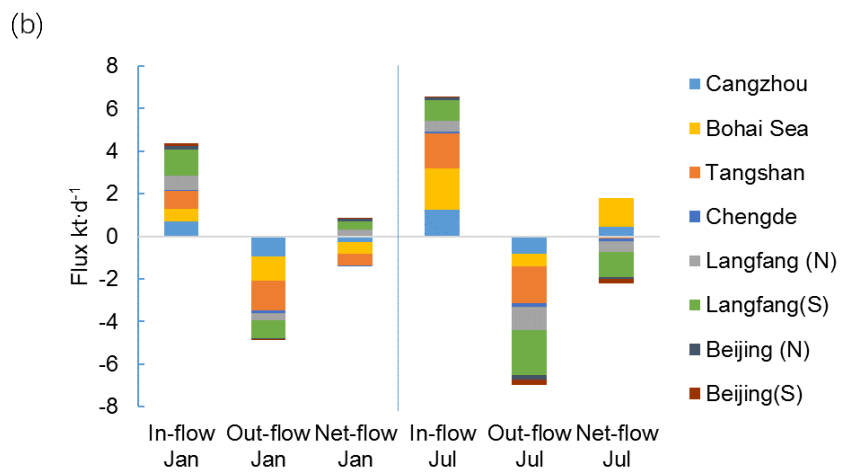
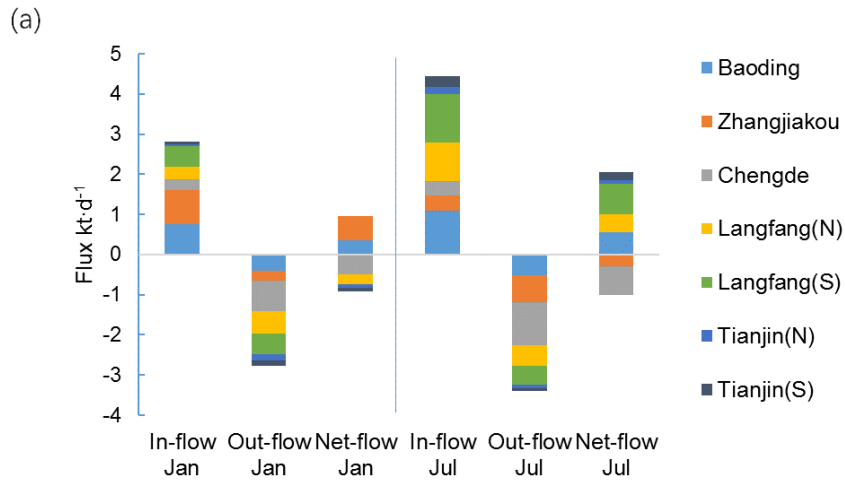
615

Figure 3 An example of the vertical surface for flux calculation (a) before discretization, and (b) after

616

discretization.

617



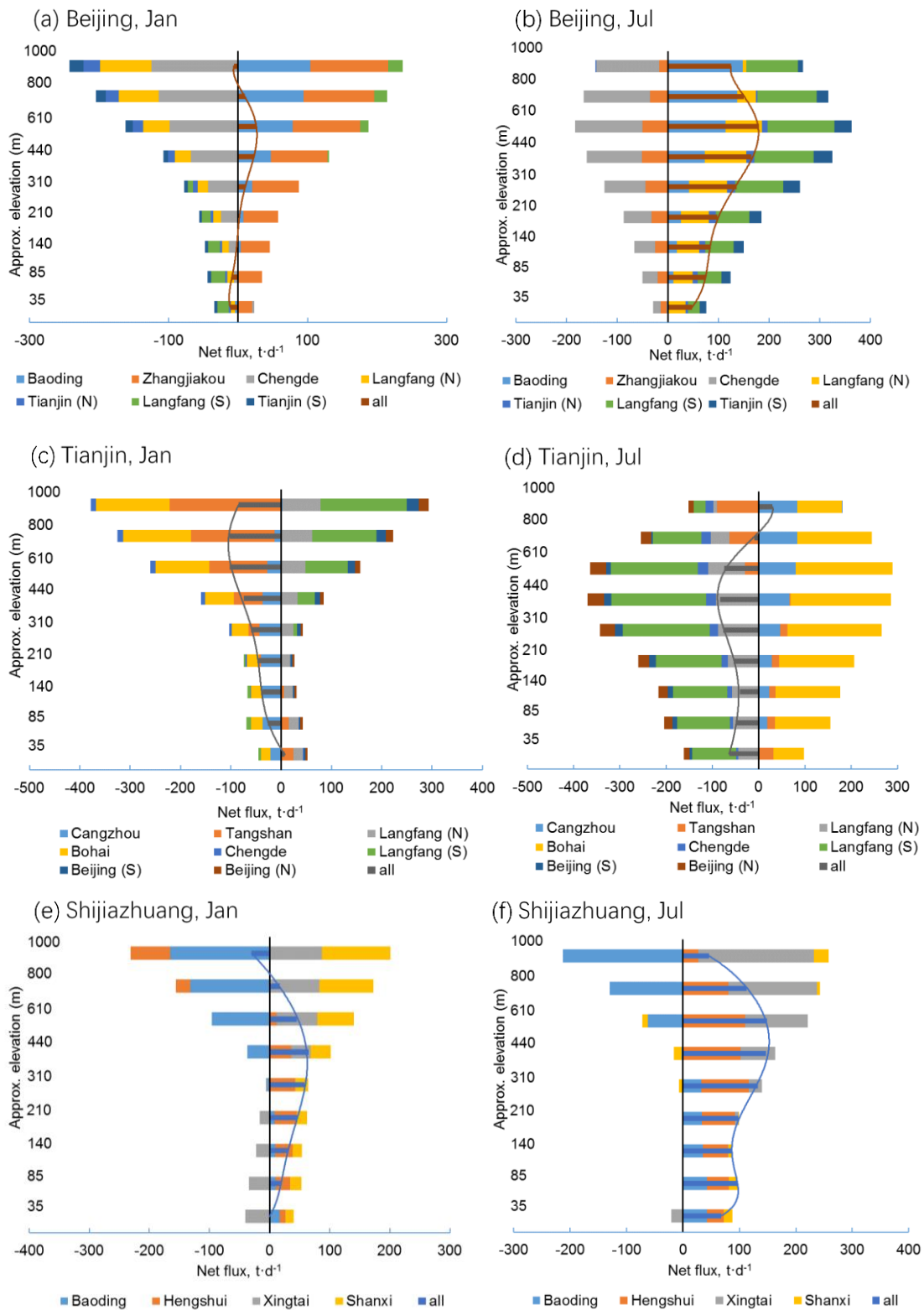
618

619

620

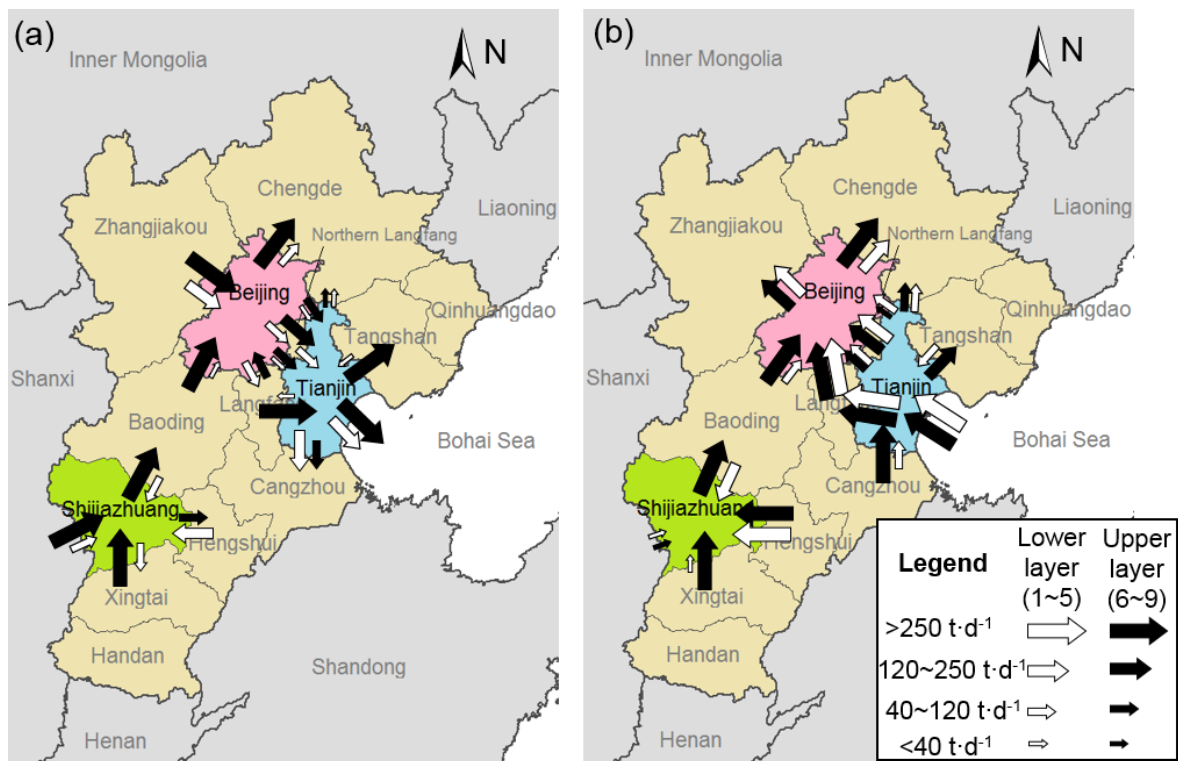
621

Figure 4 The inflow, outflow and net fluxes in January and July for (a) Beijing, (b) Tianjin, and (c) Shijiazhuang



622
623
624
625

Figure 5 Vertical distribution of net fluxes in January (left) and July (right) for (a-b) Beijing, (c-d) Tianjin, and (e-f) Shijiazhuang



626

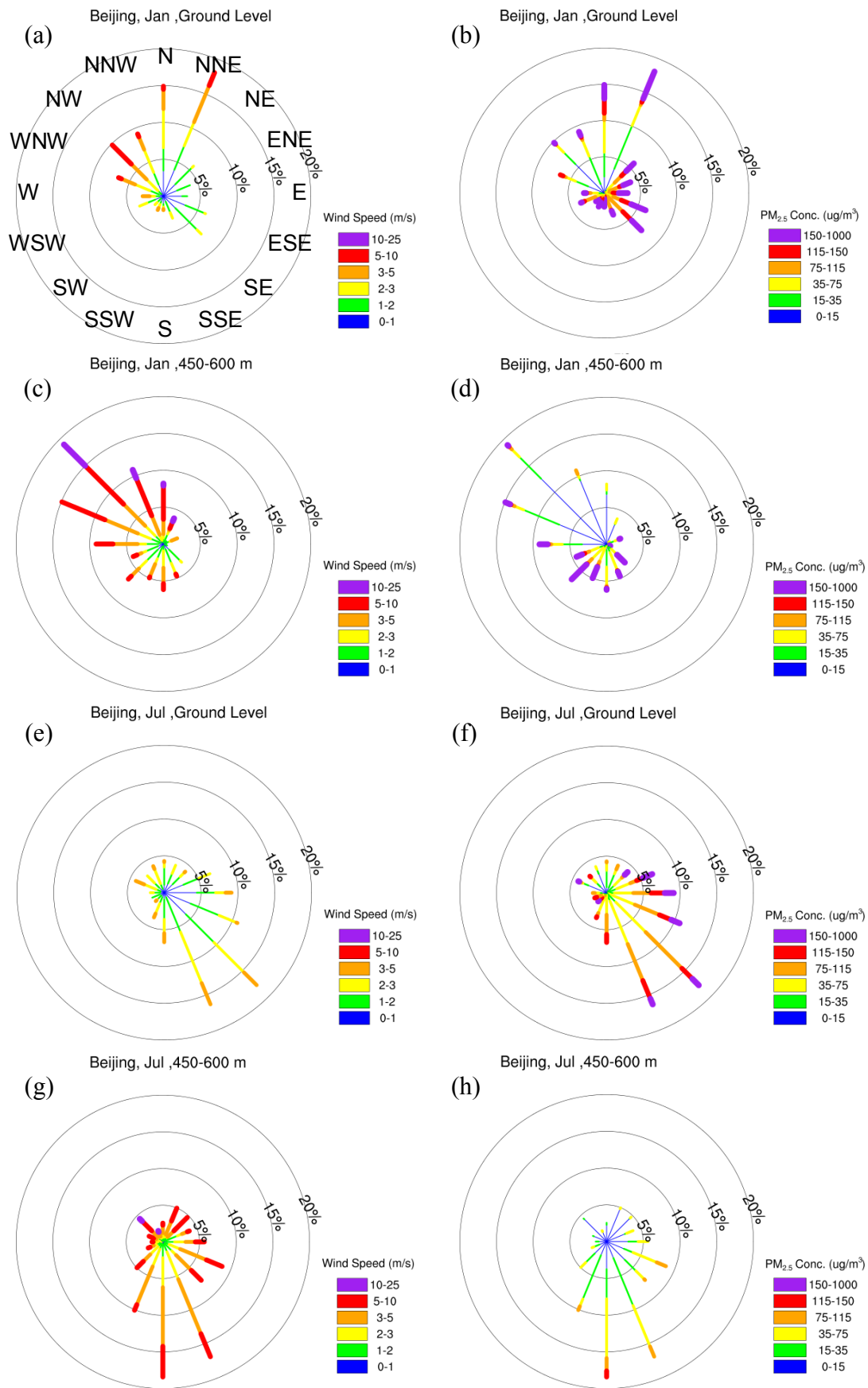
627

628

629

630

Figure 6 The transport fluxes through each boundary segment of the three target cities in January (a) and July (b). The size of the arrows represents the amount of the fluxes, while white and black arrows denote fluxes at the lower (layer 1-5 in the model, from the ground to about 310 m) and upper (layer 6-9 in the model, from about 310 m to about 1000 m) layers, respectively.

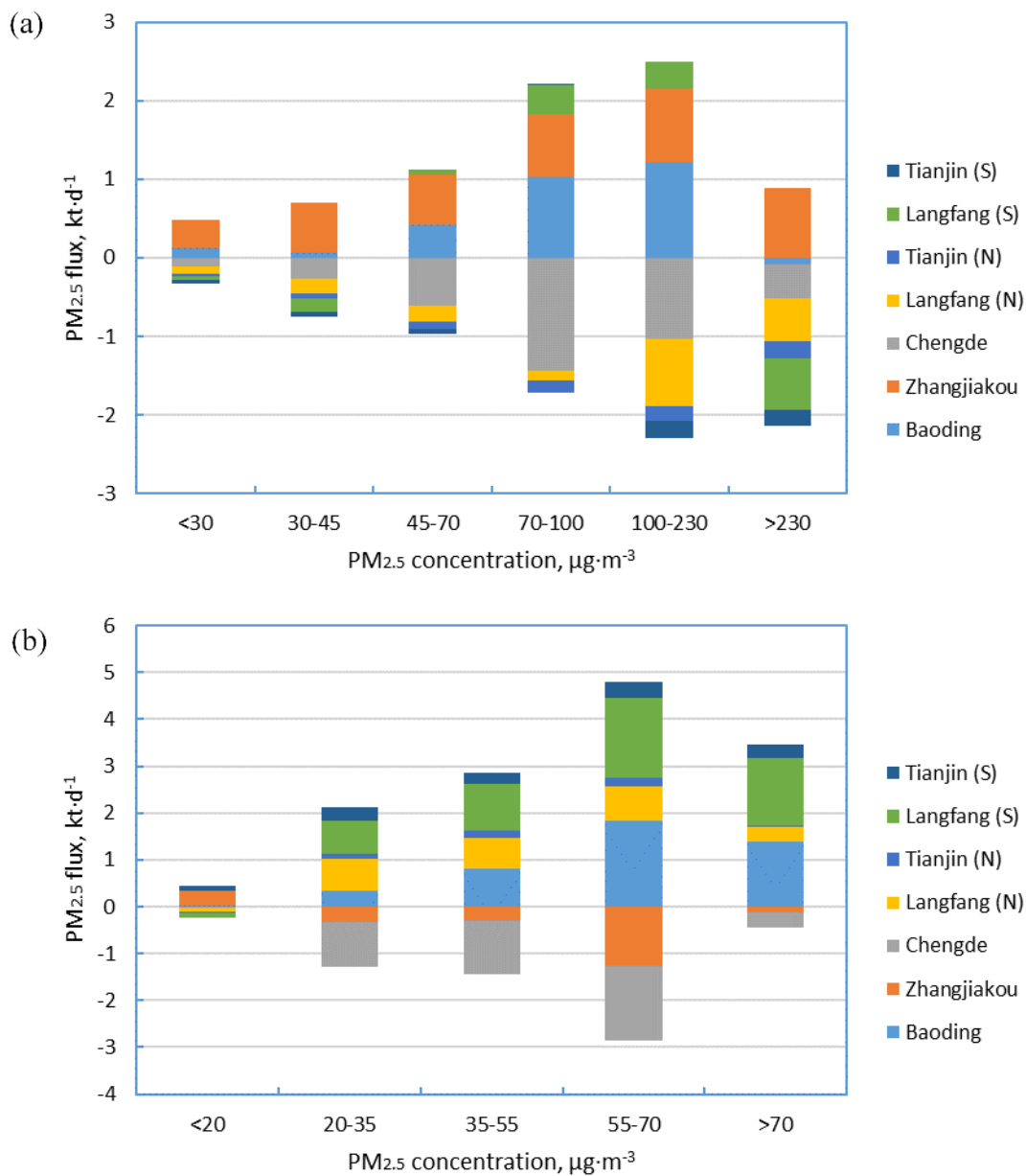


631

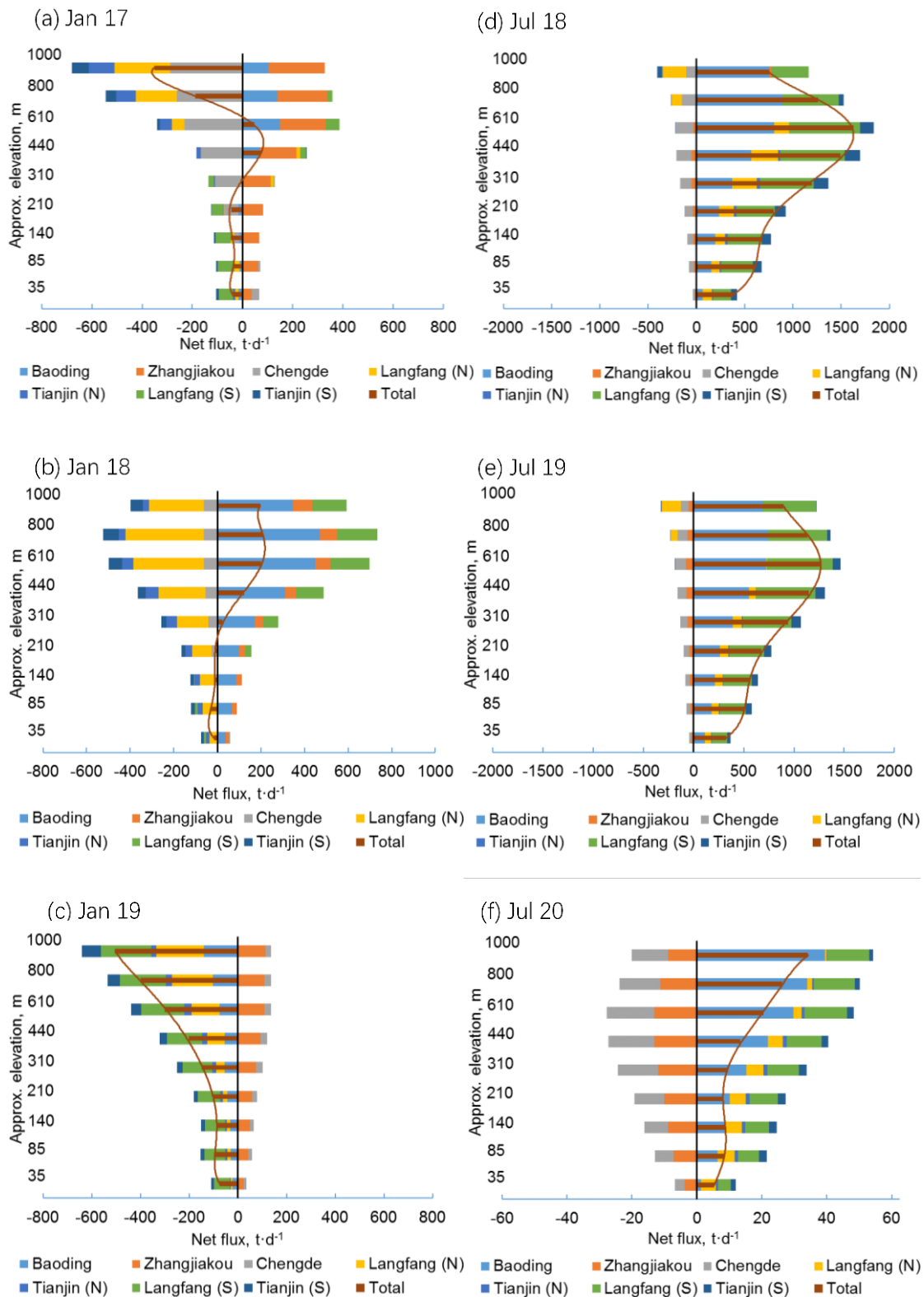
632

Figure 7 The wind rose plots showing the frequency of wind speed (a, c, e, g) and PM_{2.5} concentration

633 (b, d, f, h) at different wind directions for Beijing. The ground level and the 7th level (about 450-600 m)
 634 in the model are chosen as the representation of lower levels and upper levels. The percentages denote
 635 the frequency.
 636



637
 638 **Figure 8 PM_{2.5} average flux in different pollution degrees in (a) January and (b) July.**
 639



640

641

642

Figure 9 PM_{2.5} fluxes during heavy-pollution days in Beijing in January and July: (a) January 17th, (b) January 18th, (c) January 19th, (d) July 18th, (e) July 19th and (f) July 20th.